Journal of Catalysis **184,** 421–439 (1999)
Article ID jcat.1998.2357, available online at http://www.idealibrary.com on IDEAL®

Carbon-Supported Copper Catalysts

II. Crotonaldehyde Hydrogenation

A. Dandekar,[1] R. T. K. Baker,[2] and M. A. Vannice[3]

Department of Chemical Engineering, The Pennsylvania State University, University Park, Pennsylvania 16802

Received October 23, 1998; accepted November 30, 1998

The adsorption and catalytic behavior of Cu supported on different forms of carbons, i.e., activated carbon, graphitized carbon fibers, and diamond powder, were examined during crotonaldehyde hydrogenation. Activities as well as turnover frequencies (TOFs) varied significantly as a function of the support, the pretreatment temperature, and the catalyst preparation technique; for example, activities at 423 K ranged from 0.23 to 18 μmol/s/g cat while TOFs ranged from 0.001 to 0.13 s^{-1} after reduction at 573 K. A maximum in TOF was exhibited by each catalyst as a function the fraction of Cu^0 at the surface, i.e., $Cu^0/(Cu^0 + Cu^{+1})$, which is attributed to enhanced reactivity of crotonaldehyde adsorbed on Cu^{+1} sites. Whereas typical Cu catalysts, including Cu powder, exhibited similar TOF values after a given reduction step, significantly higher TOFs were obtained with Cu dispersed on a nitric acid-treated activated carbon; this is attributed to additional adsorption sites on the carbon surface for crotonaldehyde which allow it to react with hydrogen spilled over from Cu^0 sites. In contrast, unusually low TOFs and a higher selectivity to crotyl alcohol were exhibited by Cu deposited on the graphitized fibers by an ion-exchange technique, which may be due to small Cu particles preferentially stabilized along the edges of the graphitic basal planes. Selectivity to crotyl alcohol was routinely near zero after 3 h on stream. Both diffuse reflectance FTIR spectroscopy (DRIFTS) and kinetic data obtained during crotyl alcohol and butyraldehyde hydrogenation indicated stronger adsorption and higher reactivity of crotyl alcohol on Cu, presumably leading to these low steady-state selectivities. DRIFT spectra taken under reaction conditions revealed adsorbed crotonaldehyde, provided evidence for a monohydrogenated reactive intermediate with detectable surface coverage, and detected no adsorbed butyraldehyde. A Langmuir–Hinshelwood model incorporating this reaction intermediate gave an excellent fit of the kinetic data and provided physically meaningful values for enthalpies and entropies of adsorption.

INTRODUCTION

Carbon-supported precious metals are widely used as commercial catalysts in industrial hydrogenation and organic synthesis reactions, and the critical importance of relevant physical and chemical properties of carbons when used as supports in heterogeneous catalysts has been readily accepted (1–10). As is obvious from these review articles, because of the variety of their properties such as porosity, surface area, and chemical nature of the surface, activated carbons have played a significant role as adsorbents, catalysts, catalyst supports, and even reactants. The optimization of carbon surface chemistry to induce desirable strong interactions at the interface between the metal precursor and the support, as well as the influence of these modifications on the morphological and adsorption properties of the resulting metal particles, has received much attention (1–10). In addition to activated carbon, the application of two other forms of carbon, i.e., graphite and diamond, has also received some attention during the past few years (1, 11–46); however, whereas the morphological and electronic properties of metals dispersed on these substrates have been investigated, the consequent effects on adsorption behavior and catalytic activity have received very limited attention.

Furthermore, in spite of the industrial importance of copper-containing mixed oxides as selective hydrogenation catalysts (47, 48), fundamental studies pertaining to characterization of Cu supported on any form of carbon are not numerous (11–15, 49–57). Since the relative amounts of surface copper atoms and cuprous ions have been proposed to play an important role in the catalytic activity of these copper catalysts, of fundamental interest is to what extent the application of different types of carbon supports can affect the catalytic properties of Cu crystallites dispersed on them. In addition, two recent developments related to copper catalysts provide new incentive for a study of their behavior. The first is the issue of the disposal of commercial copper chromite catalysts, which are used in industry for selective hydrogenation of unsaturated aldehydes and

[1] Current address: Mobil Technology Company, Paulsboro, NJ 08066-0480.

[2] Current address: Chemistry Department, Northeastern University, Boston, MA 02115.

[3] To whom correspondence should be addressed.

0021-9517/99 $30.00

ketones to the corresponding unsaturated alcohols with minimal hydrogenation of unsaturated C=C bonds (47, 48, 58, 59). Because of the possibility of chromium existing as Cr^{+6}, EPA restrictions now prevent deactivated copper chromite catalysts from being used as landfill; they must either be recycled or reclaimed, and more severe restrictions could curtail their future use completely. This creates a need for inexpensive copper catalysts that could replace the older Cr-containing catalysts. The second development relates to the recent report by Li and Armor that Cu/ZSM-5 catalysts are very active for the catalytic decomposition of N_2O, which is an industrial by-product and environmental pollutant (60). Thus, there exists a potential for developing other dispersed Cu systems which could have activities equal to or greater than these zeolite systems.

Based on these considerations, Cu crystallites dispersed on three different forms of carbon, i.e., activated carbon, graphitized carbon fibers, and diamond, were prepared and characterized, and the effect of different surface and bulk properties of the carbons on catalytic behavior was examined. Characterization of these pure carbon supports using X-ray diffraction (XRD), temperature-programmed desorption TPD, and diffuse reflectance FTIR spectroscopy (DRIFTS) has been described in detail elsewhere (61). A detailed characterization of these C-supported Cu catalysts by CO chemisorption, N_2O decomposition, X-ray diffraction, transmission electron microscopy, and DRIFTS is presented in the preceding paper (62). This paper describes the adsorption and catalytic behavior of these catalysts during crotonaldehyde hydrogenation. The kinetics of N_2O decomposition over selected Cu catalysts will discussed in a subsequent publication (63).

EXPERIMENTAL

Catalyst Preparation and Characterization

Details regarding the preparation and surface characterization of these carbon-supported copper catalysts are given elsewhere (62, 64), but a brief summary follows. Activated carbon (A8933, NORIT Corp, 800 m^2/g), designated AC-ASIS, was subjected to two different pretreatments. A high-temperature treatment (HTT) in flowing H_2 at 1223 K was used to prepare the support labeled AC-HTT-H_2, while a third sample, designated AC-HNO_3, was prepared by heating AC-ASIS in 12 N nitric acid for 12 h at 363 K. The highly graphitic carbon fibers (GF) were pitch-based commercial fibers (P-25, Amoco Performance Products, 6 m^2/g). The synthetic diamond powder (DM) was obtained from Alfa Aesar (99.9+% purity, metals basis 25 m^2/g). A standard wet impregnation (WI) technique was utilized to prepare nominal 5 wt% Cu catalysts with all three activated carbons, the graphitized fibers, and the diamond powder. After aqueous impregnation at room temperature, all the catalysts, i.e., Cu/AC-ASIS, Cu/AC-HTT-H_2, Cu/AC-HNO_3 Cu/DM, and Cu/GF-WI, were dried in an oven overnight at 393 K in air. A 1.8 wt% Cu catalyst was also prepared with the graphitized fibers by an ion-exchange (IE) technique using aqueous solutions of $Cu(NO_3)_2$ and concentrated ammonia to maintain a pH of 10 according to literature procedures (23, 64). This catalyst is designated as Cu/GF-IE. In addition to the 5% catalysts and the 1.8% Cu/GF-IE sample described above, for utilization of the Madon–Boudart criterion to verify the absence of mass and heat transfer limitations (65), 1 and 10% Cu/AC-HNO_3, and 1 and 2% Cu/DM catalysts, were also prepared using the wet impregnation technique. Similarly, 0.2 and 1.3% Cu/GF-IE catalysts were also prepared using the ion-exchange technique. In the remainder of this section, unless otherwise specified, all samples designated as Cu/AC-ASIS, Cu/AC-HTT-H_2, Cu/AC-HNO_3, Cu/DM, and Cu/GF-WI will refer to catalysts with approximately 5 wt% Cu loadings, and Cu/GF-IE will refer to the ion-exchanged 1.8 wt% Cu/GF catalyst.

Prior to any adsorption or kinetic measurements, the catalyst samples were pretreated *in situ* in 40 sccm He (99.999% purity, MG Ind.) at 1 atm for 1 h at 423, 473, 573, or 673 K, followed by reduction in 40 sccm H_2 (99.999% purity, MG Ind.) for 4 h at the same temperature. As described in detail elsewhere (66), "O" uptakes on all the catalysts after the desired pretreatment were determined via N_2O decomposition at 363 K in a gravimetric apparatus and used to count the number of Cu^0 surface sites assuming Cu_2O was formed. Irreversible CO uptakes were measured at 300 K in a volumetric apparatus in order to estimate the number of Cu^{+1} sites. A UHP Cu powder (Alfa Aesar, 99.999% purity) was also used after cleaning in a flow of H_2 at 673 K for 4 h. Separate samples of Cu/AC-HNO_3 were reduced *ex situ* at either 873 or 1173 K for 1 h in a tubular quartz reactor (64), cooled to room temperature in flowing H_2, and then transferred to a N_2-purged glove box for storage. Prior to any chemisorption or catalytic runs, these samples were reduced *in situ* for 4 h at 673 K to remove any reoxidation that might have occurred during the aerobic handling and transfer of these samples. An additional catalyst sample, designated as Cu/AC-HNO_3-NH_3, was prepared by treating Cu/AC-HNO_3 with a 9 N solution of NH_4OH under constant stirring for 12 h to neutralize acid sites. The sample then was washed with distilled, deionized water, filtered, and dried overnight in air in a oven maintained at 393 K.

Hydrogenation of Crotonaldehyde

The kinetics of vapor-phase crotonaldehyde (CROALD) hydrogenation were determined at atmospheric pressure in a microreactor system described earlier (47). After loading typically 0.04–0.1 g of the catalyst sample in the reactor, it was pretreated *in situ* for 4 h at the desired pretreatment

temperature under flowing He and H_2, as mentioned earlier, and the reactor temperature was then cooled to the desired reaction temperature. Mass flow rates of H_2 and the diluent He (99.999% purity, MG Ind.) were regulated by mass flow controllers (Tylan, Model FC-260). A constant flow of vapor-phase CROALD (CH_3–CH=CH–CH=O) was established by bubbling either H_2 or He as the carrier gas through a saturator containing liquid CROALD (99.9+% purity, Aldrich). Standard conditions for activity runs were 35 Torr CROALD and ca. 710 Torr H_2, with Arrhenius plots obtained over a temperature range of 373 to 473 K for Cu/AC-HNO_3, 423 to 523 K for Cu/AC-ASIS and Cu/AC-HTT-H_2, 373 to 443 K for Cu/DM, 423 to 523 K for Cu/GF-WI, and 423 to 548 K for Cu/GF-IE. The data during the Arrhenius runs were obtained after waiting for a period of about 30 min under each set of reaction conditions to allow the system to reach stable activity. In addition, an ascending temperature sequence was followed by a descending temperature sequence to check for deactivation. Partial pressure dependencies on CROALD were obtained for Cu/AC-HNO_3, Cu/DM, Cu/GF-WI, and Cu/GF-IE between 35 and 150 Torr at a H_2 pressure of 400 Torr, while dependencies on H_2 were measured over a range of 145 to 725 Torr at a CROALD pressure of 35 Torr. The partial pressure data were acquired at three different reaction temperatures for each of these catalysts. Hydrogenation of butyraldehyde (BUTALD, 99.9+% purity, Aldrich) and crotyl alcohol (CROALC, 99.9+% purity, Aldrich) was also studied over Cu/AC-HNO_3, Cu/DM, Cu/GF-WI, and Cu/GF-IE catalysts in an identical fashion. All kinetic measurements were made at atmospheric pressure and under differential conditions as conversions were routinely maintained below 15%, except for one run with Cu/DM to determine product distribution at higher reaction temperatures where conversions approached 100%.

DRIFTS

Details of the modified diffuse reflectance FTIR reactor system used in the present study and the standard procedures employed to record the spectra have been described in detail earlier (47, 61). As before, in order to enhance the low signal-to-noise ratios typically obtained with carbon samples, all three activated carbon-supported samples were diluted with CaF_2 to give a CaF_2 : catalyst ratio of 10 : 1 before loading into the DRIFTS cell. Similarly, the graphitized fiber-supported samples were diluted with CaF_2 to give a CaF_2 : catalyst ratio of 5 : 1 prior to loading. In both cases, a lower dilution ratio yielded a very low signal-to-noise ratio, whereas a higher ratio lowered the spectrum resolution (64). The diamond powder-supported samples were analyzed without any diluent. After loading the catalyst sample into the DRIFTS reactor cell, the cell was purged overnight with Ar in order to minimize additional signal damping caused by ambient moisture. The sample was then subjected to *in situ* pretreatment at the desired temperature and cooled to 300 K, at which point the first interferogram was recorded. This was used as a background reference in the fast Fourier transform analysis of all the subsequent interferograms recorded for that particular catalyst. The sample temperature was then raised to the desired reaction temperature, and a mixture of 370 Torr H_2 and 15 Torr CROALD was introduced into the cell. The mixture was obtained by bubbling 50% H_2 in He (20 sccm) through CROALD maintained at 273 K in an ice bath. Spectra were recorded for each catalyst under these reaction conditions at the desired reaction temperature.

In order to investigate CROALD adsorption on Cu in different oxidation states, a 15 Torr mixture of CROALD in Ar was flowed at 423 K over the 5% Cu/DM catalyst after one of three different pretreatments: (I) calcination in 20% O_2/Ar at 573 K for 4 h, (II) reduction in H_2 at 673 K for 4 h, and (III) reduction in H_2 at 673 K for 4 h followed by reoxidation in 75 Torr N_2O at 363 K for 30 min to give only Cu^{+1} sites at the surface.

Spectra of BUTALD and CROALC adsorbed on Cu/DM at 423 K after reduction at 573 K were also obtained in a similar fashion by flowing 30 and 10 Torr mixtures, respectively, of these reagents over these catalysts with Ar (20 sccm) as a carrier gas. In addition, vapor-phase spectra of CROALD, BUTALD, and CROALC were obtained at 423 K by passing 15, 30, and 10 Torr mixtures, respectively, of these reagents in Ar (20 sccm) over an aluminum mirror placed in the reactor cell. These spectra were used to subtract out the gas-phase contributions while analyzing the *in situ* spectra of these reagents under reaction conditions.

RESULTS

The steady-state activities and TOFs at 423 K as well as the activation energies for CROALD hydrogenation over various Cu catalysts after different pretreatments are shown in Table 1, along with Cu^0 and Cu^{+1} concentrations determined by "O" and CO uptakes, respectively (62). Substantial evidence has been presented earlier that "O" and CO chemisorption summed together represent a valid approach to counting the total number of surface Cu^0 and Cu^{+1} sites after a given pretreatment (62, 66). The TOFs in Table 1 are therefore based on the sum of the individual amounts of surface Cu^0 and Cu^{+1} sites obtained by assuming a stoichiometry of 2 : 1 for Cu : O and 1 : 1 for Cu : CO. The initial and steady-state selectivities at 423 K for crotyl alcohol, i.e., (mol CROALC)/(mol CROALC + mol BUTALD), over all the catalysts are also listed in Table 1. No formation of *n*-butanol (BUTNOL) was observed over any of the catalysts at 423 K. As seen in Table 1, a wide variation in the activities and TOFs occurred depending on the support and reduction temperature as well as the catalyst preparation technique.

TABLE 1

Crotonaldehyde Hydrogenation over Cu Catalysts; $P_{CROALD} = 35$ Torr, $T = 423$ K

Catalyst	T_{RED} (K)	Surface Cu^{+1} (μmol CO/g)	Surface Cu^0 (μmol O/g × 2)	Activity (μmol/g/s)[a]	TOF (s^{-1})[b]	E_{ACT} (kcal/mol)	S (%)[c]	S^d
4.8% Cu/AC-HNO_3	423	52	220	32.1	0.12	10.3 ± 0.4	3.2	0
	473	25	154	22.6	0.12	11.0 ± 0.6	2.5	0
	573	10	112	18.4	0.13	11.6 ± 0.6	3.1	0
	673	0	99	8.9	0.09		2.2	0
	873	—	67	3.4	0.05		3.5	0
	1173	—	41	1.3	0.03		3.9	0
4.8% Cu/AC-ASIS	423	89	0	0	0	—	—	—
	573	25	110	1.6	0.012	10.9 ± 1.1	3.1	0
	673	0	102	1.1	0.01	11.2 ± 0.8	1.8	0
4.8% Cu/AC-HTT-H_2	423	22	0	0	0	—	—	—
	573	20	84	1.1	0.01	11.8 ± 1.2	4.1	0
	673	0	75	0.7	0.009	12.5 ± 1.0	2.8	0
5% Cu/DM	423	55	0	0	—	—	—	—
	473	45	38	2.5	0.026	15.2 ± 1.0	2.5	0
	573	35	50	2.7	0.03	16.2 ± 0.7	3.1	0
	673	10	70	2.1	0.028	15.5 ± 1.2	1.2	0
5.1% Cu/GF-WI	423	5	0	0	0	—	—	—
	473	7	0	0	0	—	—	—
	573	6	3	0.3	0.03	18.3 ± 1.2	1.5	0
	673	5	5	0.2	0.02	19.6 ± 1.1	2.1	0
1.8% Cu/GF-IE	423	25	82	0	0	—	—	0
	473	0	110	0	0	—	—	0
	573	0	128	0.23	0.001	23.9 ± 1.5	15.1	9.0
	673	0	62	0.14	0.002	24.2 ± 1.2	12.7	7.8
Cu powder	673	0	11.8	0.3	0.025	19.9 ± 1.2	0	0
Cu/AC-HNO_3-NH_3	423	43	115	6.2	0.039	—	1.9	0
	573	21	81	2.5	0.024	—	3.1	0

[a] Based on steady-state crotonaldehyde disappearance.
[b] Based on $Cu^0 + Cu^{+1}$ sites.
[c] Selectivity, CROALC/(CROALC + BUTALD), after 30 min.
[d] Selectivity, CROALC/(CROALC + BUTALD), after 180 min.

Representative activity maintainence profiles based on BUTALD and CROALC formation for all three AC catalysts, i.e., Cu/AC-HNO_3, Cu/AC-ASIS, and Cu/AC-HTT-H_2, after reduction at 573 K along with that for unsupported Cu powder are shown in Fig. 1. Those for Cu/DM, Cu/GF-WI, and Cu/GF-IE catalysts are provided elsewhere (64). Deactivation to some extent was evident for all catalysts; however, once steady state was reached, the activities were relatively constant for long periods of time. Each catalyst except Cu/GF-IE exhibited a consistently low initial selectivity for CROALC which rapidly dropped to nondetectable levels during the first 60 min on stream. With Cu/GF-IE, an initial selectivity of 15% was obtained, which decreased to about 9% over a period of 3 h.

Representative Arrhenius plots are shown for the three AC-supported catalysts after reduction at 573 K in Fig. 2, along with that for the unsupported Cu powder. All Cu/AC catalysts had mean activation energies of 11.5 ± 1.0 kcal/mol, which are higher than those reported earlier for copper chromite (47). Corresponding Arrhenius plots for Cu/DM, Cu/GF-WI, and Cu/GF-IE are provided elsewhere (64). Whereas the activation energies for Cu/DM and Cu/GF-WI approached the value of 20 kcal/mol for Cu powder, those for Cu/GF-IE were about 4 kcal/mol higher. In all cases, however, the activation energies for a given catalyst did not vary significantly as a function of the pretreatment temperature employed.

As seen in Table 1, Cu/AC-HNO_3 provides both the highest activity per gram at 423 K and the largest TOF after reduction at 423 K, but they both steadily dropped by a factor of almost 4 as the reduction temperature was increased to 673 K. In contrast, both Cu/AC-ASIS and Cu/AC-HTT-H_2 exhibited no detectable activity after reduction at 423 K, and both the activity and the TOF for either catalyst after higher temperature reductions were much lower than the corresponding values for Cu/AC-HNO_3. The activity

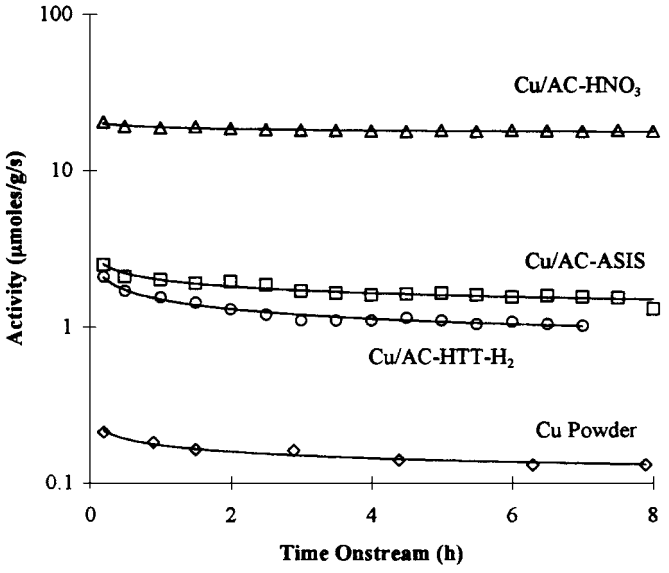

FIG. 1. Activity maintenance profiles of Cu/AC-HNO_3, Cu/AC-ASIS, Cu/AC-HTT-H_2, and Cu powder after reduction at 573 K; $T_{RXN} =$ 423 K.

of Cu/DM was almost twice as high as that of Cu/AC-ASIS or Cu/AC-HTT-H_2; however, TOFs were comparable. Similar TOFs are also observed in the case of Cu/GF-WI, although activities are much lower than those of Cu/DM. The TOF on unsupported Cu powder, based on surface metallic Cu atoms, is also in close agreement with TOF values for Cu/AC-ASIS, Cu/AC-HTT-H_2, Cu/DM, and Cu/GF-WI after high-temperature pretreatments. In contrast, the TOFs on Cu/GF-IE are an order of magnitude lower than those on the aforementioned group of catalysts, irrespective of the pretreatment temperature. It should also be noted that

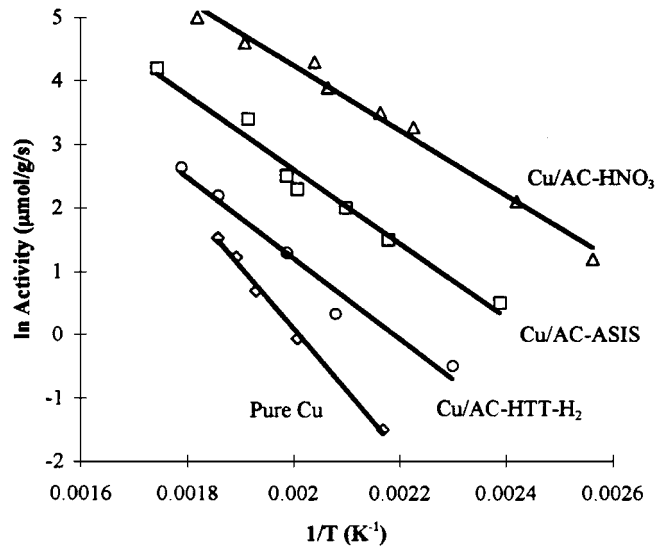

FIG. 2. Arrhenius plots for Cu/AC-HNO_3, Cu/AC-ASIS, Cu/AC-HTT-H_2, and Cu powder after reduction at 573 K.

no detectable activity was exhibited by either of the two GF catalysts after reduction at either 423 or 473 K.

Figure 3 compares TOFs on all catalysts at 423 K as a function of the reduction temperature; note that TOFs are plotted on a logarithmic scale. It is obvious from Fig. 3 that, *irrespective of the pretreatment temperature employed*, Cu/AC-HNO_3 exhibits TOFs which are 4–8 times higher than those for Cu/AC-ASIS, Cu/AC-HTT-H_2, Cu/DM, Cu/GF-WI, and Cu powder. In contrast, TOFs observed on Cu/GF-IE are an order of magnitude lower than those exhibited by this latter group. If it is presumed that the TOFs exhibited by this group of five catalysts represent typical values on unpromoted Cu, then the behavior exhibited by Cu/AC-HNO_3 and Cu/GF-IE clearly deviates from the expected pattern and suggests that the support can play a significant role in modifying the inherent properties of Cu catalysts. As shown in Table 1, the TOFs on Cu/AC-HNO_3 are maximized after reduction at 573 K, and reduction at higher temperatures leads to a rapid drop, with the TOF after reduction at 1173 K being one-fourth that of the maximum value. A distinct trend in the TOF behavior of the "typical" Cu catalysts is also apparent; i.e., whereas no activity is detected with any of the catalysts after reduction at 423 K, the TOFs for each catalyst are maximized after reduction at 573 K.

Both the Madon–Boudart test (65) and the Weisz–Prater criterion were used to check for diffusional limitations in each of the catalysts. The average pore sizes used for the calculation of the Weisz–Prater parameter were obtained from a pore-size analysis of these carbon supports conducted in a parallel study (68). The Weisz–Prater values were far below 0.3 in all cases, i.e., 2×10^{-6} to 6×10^{-3}, thus indicating the absence of significant diffusional limitations (64). Table 2 shows the results from the Madon–Boudart test used to check for mass and heat transfer limitations

TABLE 2

Madon–Boudart Test for Diffusional Limitations (65)

Catalyst[a]	Cu loading (wt%)	d_{Cu} (nm)[b]	Surface Cu (μmol/g)[b]	Activity (μmol/g/s)[c]	E_{ACT} (kcal/mol)	Slope
Cu/AC-HNO_3	1	5.2	34	5.4	10.9	0.93
	5	6.1	144	18.4	11.6	0.92
	10	7.8	227	33.1	10.5	0.88
Cu/DM	1	9.5	19	1.1	14.4	0.92
	2	11.4	32	1.5	15.6	1.05
	5	11.0	85	2.7	16.2	1.01
Cu/GF-IE	0.2	2.9	34	0.10	23.6	1.00
	1.3	3.1	74	0.15	22.5	1.06
	1.8	2.5	128	0.23	21.9	1.03

[a] Reduced at 573 K.
[b] Based on sum of CO and "O" uptakes ($Cu^{+1} + Cu^0$).
[c] Based on CROALD consumption at 423 K.

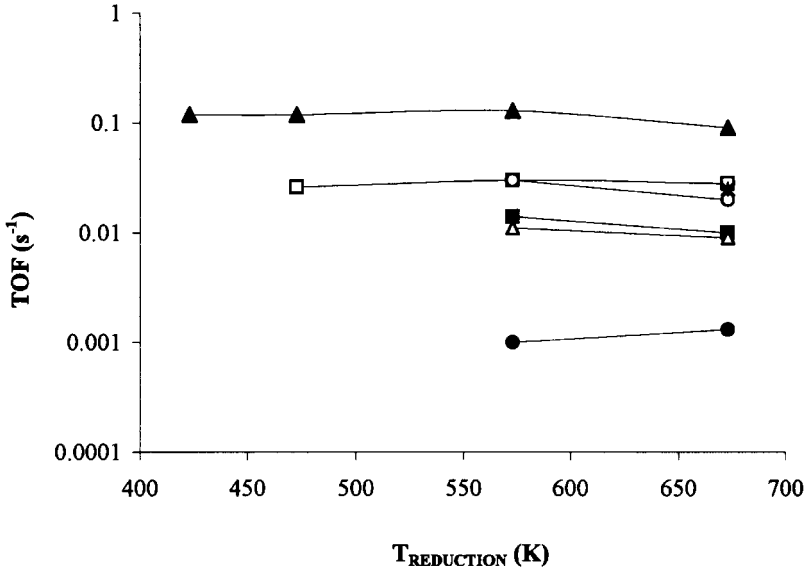

FIG. 3. TOFs for crotonaldehyde hydrogenation over all Cu catalysts vs reduction temperature; $T_{RXN} = 423$ K. (▲) AC-HNO_3; (■) AC-ASIS; (△) AC-HTT-H_2; (□) DM; (○) GF-IW; (∗) Cu; (●) GF-IE.

during CROALD hydrogenation on Cu supported on AC, DM, and GF. As discussed earlier, the CO uptake and the "O" uptake via N_2O decomposition are used to estimate the total surface concentration of Cu sites. A typical set of Arrhenius plots is shown in Fig. 4A for 1, 2, and 5% Cu/DM, and the logarithm of the reaction rate at three reaction temperatures is plotted vs the logarithm of surface concentration of total Cu sites in Fig. 4B. Similar plots are shown elsewhere for the other samples (65). In all figures the slope of ln(rate) vs ln(Cu site conc.) plots is close to unity, as indicated by the values given in Table 2, thus verifying the absence of any artifacts due to heat or mass transport limitations with the Cu/DM and Cu/GF catalysts, and indicating minimal limitations with Cu/AC-HNO_3 (65).

Partial pressure dependencies during CROALD hydrogenation were obtained with Cu/AC-HNO_3 reduced at 423 K, and data were obtained at 343, 373, and 423 K to facilitate kinetic modeling, as shown in Fig. 5. Similarly, partial pressure dependencies were determined for 5% Cu/DM, 5% Cu/GF-WI, and Cu/GF-IE catalysts after reduction at 573 K. The power rate law reaction orders with respect to H_2 and CROALD were obtained for all catalysts and are listed in Table 3. The data indicate a one-half to first-order dependency on H_2 and a negative dependency on CROALD from near zero to one-half for all catalysts.

To gain more information about the reaction pathways involving CROALD, BUTALD, and CROALC hydrogenation on Cu/AC-HNO_3, Cu/DM, Cu/GF-WI, and Cu/GF-IE catalysts were also studied after reduction at 573 K. Whereas BUTALC was the only product detected during BUTALD hydrogenation over all the catalysts, both BUTALD and BUTALC were obtained during CROALC

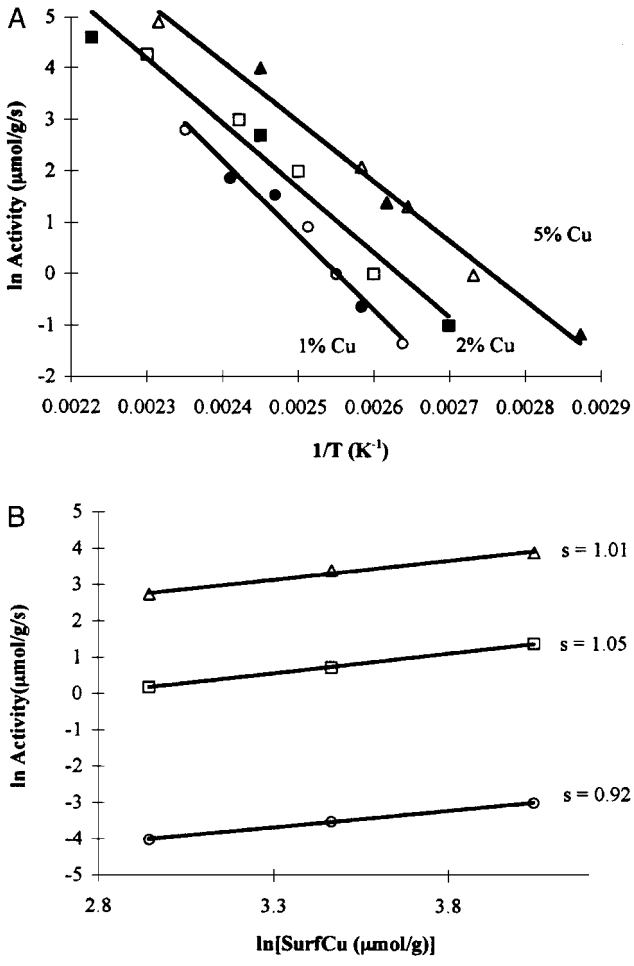

FIG. 4. (A) Arrhenius plots for 1, 2, and 5% Cu/DM. (B) Plots of specific activity vs site density.

TABLE 3

Reaction Orders for Crotonaldehyde Hydrogenation over Cu Catalysts; $T_{RED} = 573$ K

Catalyst	Reaction temp. (K)	Reaction order	
		H_2	CROALD
Cu/AC-HNO_3	343	0.61	−0.24
	373	0.58	−0.24
	423	0.57	−0.29
Cu/DM	398	0.62	−0.24
	423	0.52	−0.23
	473	0.56	−0.18
Cu/GF-WI	423	0.39	−0.58
	473	0.45	−0.46
	498	0.91	−0.37
Cu/GF-IE	473	0.73	−0.34
	498	0.74	−0.21
	523	0.57	−0.04

TABLE 4

Hydrogenation of Butyraldehyde to *n*-Butyl Alcohol over Supported Cu ($T_{RED} = 573$ K; $P_{BUTALD} = 42$ Torr; $T_{RXN} = 423$ K)

Catalyst	Activity (μmol BUTALD/g/s)	TOF (s^{-1})	E_{ACT} (kcal/mol)
Cu/AC-HNO_3	0.8	0.0066	13.9
Cu/DM	0.03	0.0004	16.9
Cu/GF-WI	0.008	0.0009	20.1
Cu/GF-IE	0.09	0.0007	15.9

hydrogenation under the reaction conditions used here. Table 4 compares the kinetic behavior of these four Cu catalysts during BUTALD hydrogenation, and the corresponding Arrhenius plots for BUTALC formation are shown in Fig. 6. The activities and TOFs of these catalysts for both CROALC hydrogenation to BUTALC and isomerization to BUTALD are listed in Table 5, and Arrhenius plots for the formation of BUTALC and BUTALD are shown in Fig. 7. As with CROALD hydrogenation, the TOFs for these reactions are markedly higher on Cu/AC-HNO_3 and lower on Cu/GF-IE compared to the Cu/DM and Cu/GF-WI catalysts. For each catalyst, the activation energy for BUTALD hydrogenation to BUTALC was similar to that observed during CROALD hydrogenation; however, the activation energies for isomerization of CROALC to BUTALD were much lower compared to those for hydrogenation to BUTALC for all catalysts except Cu/GF-IE.

The DRIFT spectra of Cu/DM after reduction at 423, 473, 573, or 673 K, recorded *in situ* under reaction conditions with 370 Torr H_2 and 15 Torr CROALD at 423 K, are

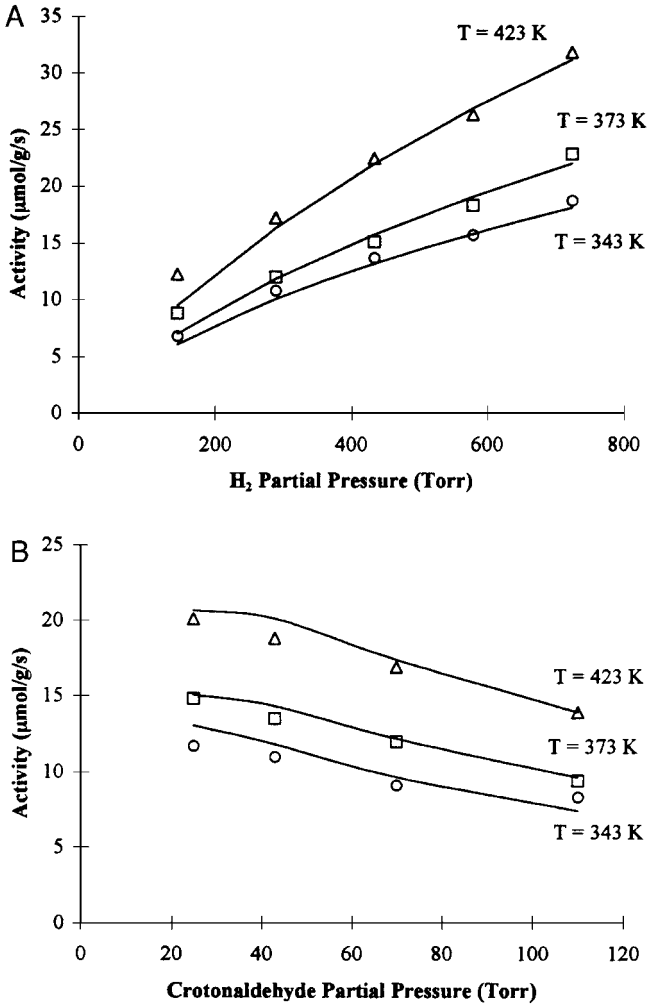

FIG. 5. Partial pressure data over Cu/AC-HNO_3 reduced at 573 K; symbols represent experimental data, whereas lines denote predicted rates.

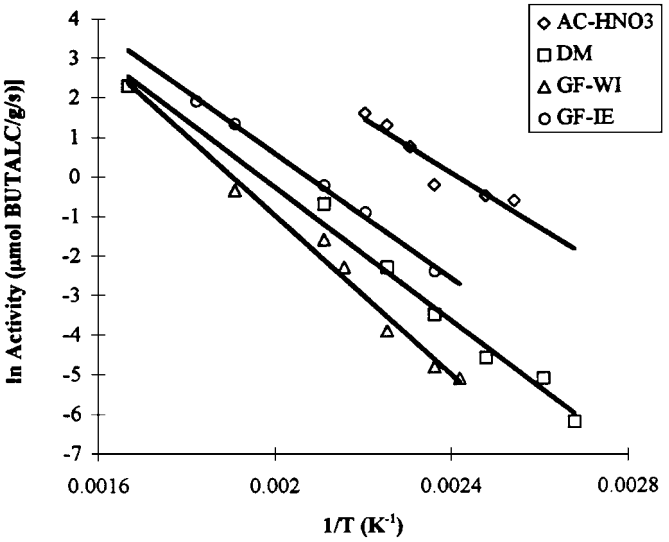

FIG. 6. Arrhenius plots for BUTALD hydrogenation to BUTALC over (◇) Cu/AC-HNO_3, (□) Cu/DM, (△) Cu/GF-WI, and (○) Cu/GF-IE reduced at 573 K.

TABLE 5

Hydrogenation of Crotyl Alcohol over Supported Cu ($T_{RED} = 573$ K; $P_{CROALC} = 35$ Torr; $T_{RXN} = 423$ K)

	Isomerization to BUTALD			Hydrogenation to BUTALC		
Catalyst	Activity (μmol/g/s)	TOF (s^{-1})	E_{ACT} (kcal/mol)	Activity (μmol/g/s)	TOF (s^{-1})	E_{ACT} (kcal/mol)
Cu/AC-HNO_3	14.5	0.12	1.0	7.2	0.06	9.8
Cu/DM	1.6	0.018	3.6	0.4	0.005	14.2
Cu/GF-WI	0.15	0.016	5.9	0.05	0.005	19.5
Cu/GF-IE	0.1	0.0008	14.5	0.15	0.0012	16.2

shown in Fig. 8. The vapor-phase spectrum of CROALD has been subtracted from these spectra. In all cases, a sharp peak developed at 1701 cm^{-1} along with weaker peaks at 970 and 1150 cm^{-1} and two broader bands near 1432 and 1541 cm^{-1}. In addition, weak absorption bands can be seen between 2730 and 3030 cm^{-1}. Reduction at 573 or 673 K shifts the position of the 1541 cm^{-1} band first to 1568 cm^{-1} and then to 1602 cm^{-1} after the higher temperature treatment. Similar DRIFT spectra of Cu/AC-HNO_3, Cu/GF-WI, and Cu/GF-IE were also obtained under identical reaction conditions (not shown); however, the spectra were not as well resolved and informative as those for Cu/DM, which is undoubtedly a manifestation of the much lower spectral resolution obtained with the *diluted* samples of these AC- and GF-supported Cu catalysts. A strong absorption peak was observed at 1703 ± 2 cm^{-1} in all cases, along with a broader band between 1540 and 1630 cm^{-1} whose intensity and position were dependent upon the reduction temperature. Several additional peaks are detected at 970, 1150, 1432, 2730, 2820, 2920, 2978, and 3026 cm^{-1} in the spectra of Cu/DM which cannot be clearly resolved in the spectra of the other three catalysts; however, the latter spectra do not disallow the possibility that some of these features are present as very weak bands. Consequently, band assignments for Cu/DM have been made on the basis of the available literature (69–74) and generalized to other catalysts when applicable, and these are discussed in the next section.

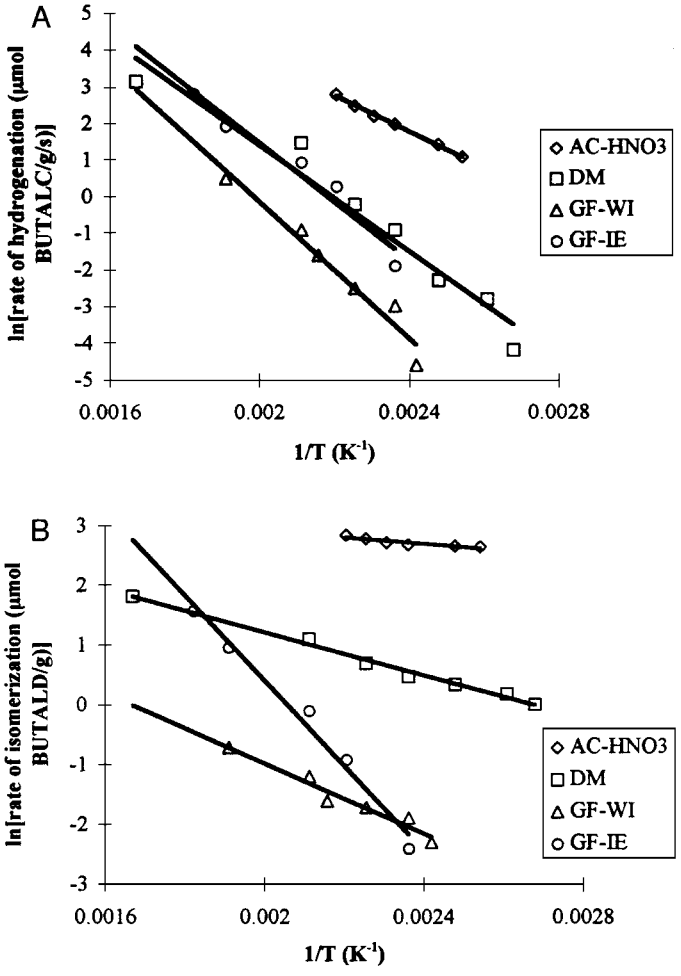

FIG. 7. Arrhenius plots for (A) CROALC hydrogenation to BUTALC and (B) CROALC isomerization to BUTALD over (◇) Cu/AC-HNO_3, (□) Cu/DM, (△) Cu/GF-WI, and (○) Cu/GF-IE catalysts reduced at 573 K.

To gain additional insight into the interaction of CROALD on the different oxidation states of Cu, CROALD adsorption at 423 K was studied on Cu/DM samples subjected to different pretreatments in order to yield surfaces consisting entirely of Cu^{+2}, Cu^{+1}, or Cu^0 species alone. The corresponding DRIFT spectra of CROALD adsorbed on these catalyst surfaces, after subtracting the gas-phase CROALD spectrum, are shown in Fig. 9. DRIFT spectra of CROALC and BUTALD adsorbed at 423 K on Cu/DM after reduction at 573 K, along with the corresponding vapor-phase spectra, are shown in Figs. 10 and 11, respectively, and are discussed in the next section.

DISCUSSION

The development and characterization of catalysts for selective hydrogenation of unsaturated aldehydes, such as CROALD, have been the focus of many studies to date,

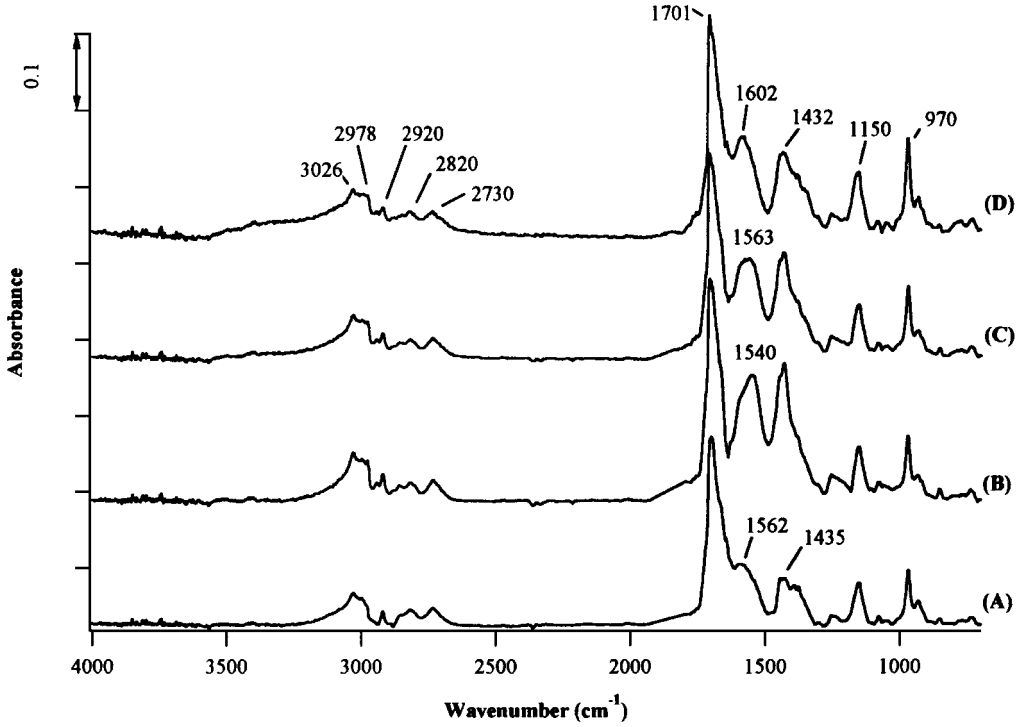

FIG. 8. DRIFTS spectra collected during crotonaldeyde hydrogenation at 423 K over Cu/DM pretreated at (A) 423 K, (B) 473 K, (C) 573 K, and (D) 673 K.

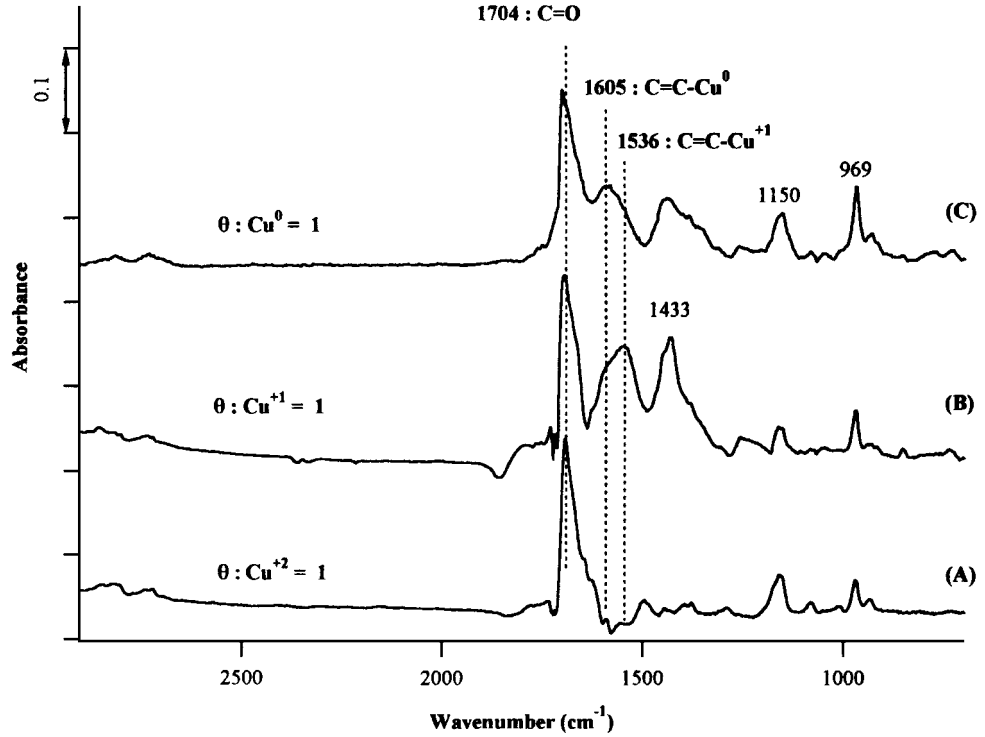

FIG. 9. DRIFTS spectra of crotonaldehyde adsorption on Cu/DM after: (A) calcination in 20% O_2/Ar at 573 K, (B) reduction at 673 K and reoxidation by N_2O at 363 K, and (C) reduction at 673 K; $P_{CROALD} = 15$ Torr.

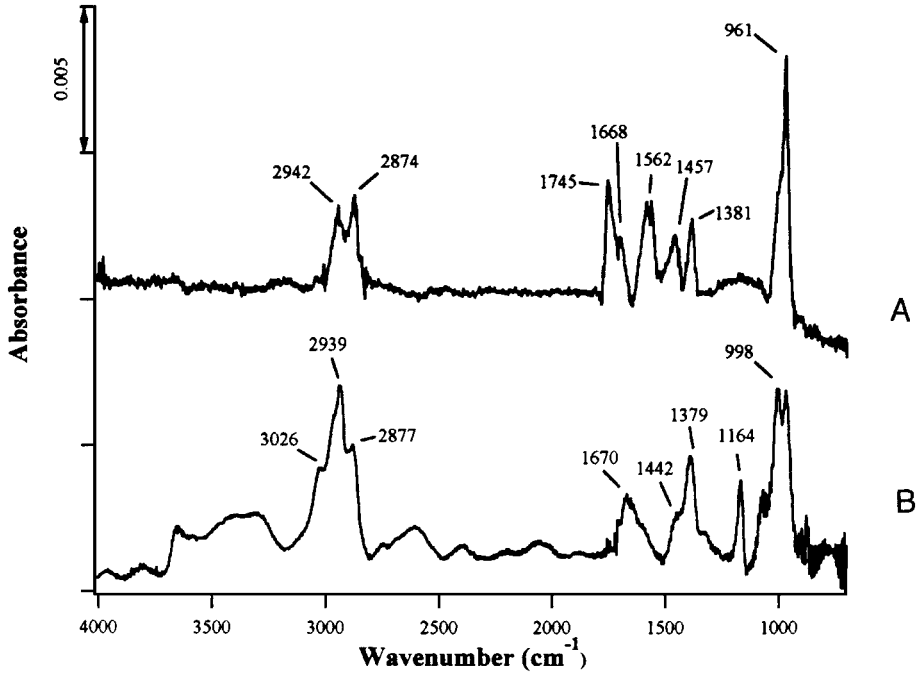

FIG. 10. DRIFTS spectra of (A) CROALC adsorbed on Cu/DM pretreated at 573 K and (B) vapor-phase CROALC; $P_{CROALC} = 10$ Torr.

and both unpromoted and promoted metals dispersed on a variety of supports have been extensively investigated (75–99). Very few studies, however, have dealt with supported copper as a hydrogenation catalyst for these reactions. Although the effects of promoting Cu with other metals like Ni (76) and nonmetal additives like Cl (77) and S (78, 79) in order to enhance selectivity have been discussed, no detailed kinetic investigation of CROALD hydrogenation over unpromoted Cu could be found in the literature. Three different active phases have been proposed in copper hydrogenation catalysts: Cu^{+1}, Cu^{0}, and a combination of these two sites. One of the principal objectives of this project,

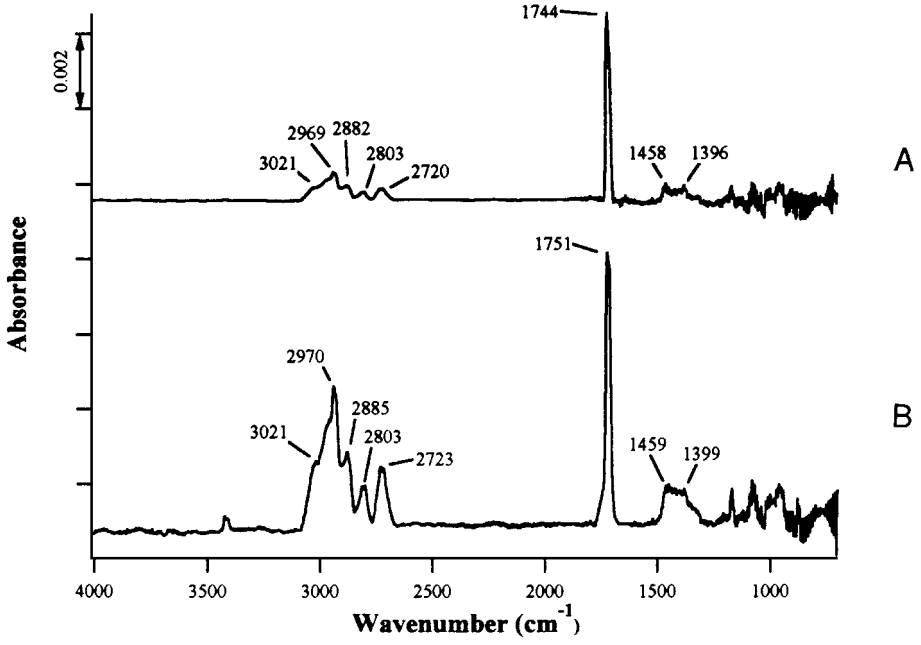

FIG. 11. DRIFTS spectra of (A) BUTALD adsorbed on Cu/DM pretreated at 573 K and (B) vapor-phase BUTALD; $P_{BUTALD} = 30$ Torr.

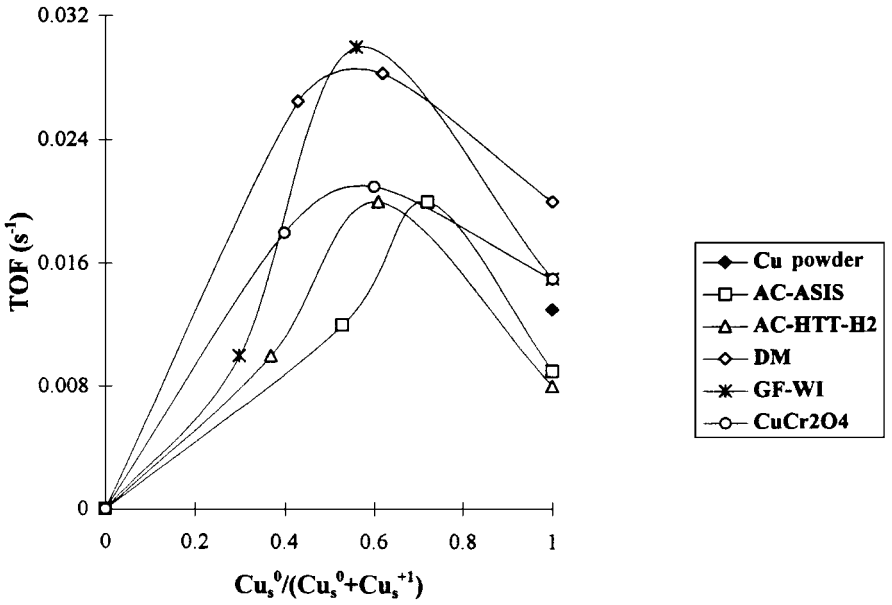

FIG. 12. Turnover frequencies, based on $Cu^0 + Cu^{+1}$ sites, of Cu catalysts vs surface fraction of Cu^0; $T_{RXN} = 423$ K, $P_{CROALD} = 35$ Torr, $P_{H_2} = 710$ Torr. (◆) Cu powder; (□) AC-ASIS; (△) AC-HTT-H_2; (◇) DM; (∗) GF-WI; (○) $CuCr_2O_4$.

therefore, was to address the controversial issue regarding the active phase(s) of Cu. As discussed previously (62), Cu dispersed on different carbons provides a set of catalysts with widely varying Cu crystallite sizes and distributions of Cu oxidation states, thereby allowing manipulation of the number and nature of surface Cu sites present during CROALD hydrogenation. Utilization of carbons with diverse surface and bulk properties as catalyst supports also grants an opportunity to investigate whether the catalytic performance of Cu in hydrogenation reactions could be modified by any metal–carbon interactions.

Table 1 illustrates the variation in turnover frequencies on Cu/AC-ASIS, Cu/AC-HTT-H_2, Cu/DM, and Cu/GF-WI catalysts as the reduction temperature is increased from 423 to 673 K. In each case, the TOF is maximized around 573 K, which is in agreement with the earlier study of copper chromite (47) and may indicate that the same active phases of Cu are involved in these reactions. Coincidence of the highest specific activity at a similar Cu^{+1} concentration provides strong evidence for the active involvement of this cation in the catalytic cycle on copper chromite, in agreement with previous conclusions. With activation of H_2 more likely to occur on Cu^0 surfaces, a synergistic effect between Cu^0 and Cu^{+1} sites was proposed to be responsible for achieving the optimum activity after pretreatment at 573 K (47); however, the concentration of each individual Cu surface species was not ascertained during this study of copper chromite. As discussed in the preceding paper (62), DRIFT spectra of CO adsorbed at 173 K on pretreated catalyst surfaces, combined with selective chemisorption, provided a convenient *in situ* analytical approach to determine the fractions of the surface composed of Cu^0 and Cu^{+1} sites after a particular pretreatment. The fractions of these Cu species were obtained for all the carbon-supported catalysts studied here after the chosen reduction step. The turnover frequencies obtained over the five "typical" catalysts, i.e., Cu/AC-ASIS, Cu/AC-HTT-H_2, Cu/DM, Cu/GF-WI, and Cu powder, are replotted in Fig. 12 versus the corresponding fraction of Cu^0 at the Cu surface. To obtain a valid comparison with Cu chromite, DRIFT spectra were also obtained of CO adsorbed at 173 K on $CuCr_2O_4$ after reduction at 473, 573, and 673 K, and the fraction of Cu^0 at the surface after each pretreatment was determined. The TOFs on $CuCr_2O_4$ based on the sum of $Cu^0 + Cu^{+1}$ sites, are also included in Fig. 12.

Figure 12 clearly illustrates the trend in the catalytic activity of Cu as the fraction of surface Cu^0 sites (θ_{Cu^0}) varies from 0 to 1. No activity is evident when θ_{Cu^0} is zero, clearly implying that the presence of some metallic Cu is absolutely essential for an active catalyst; however, TOFs are still significant when only Cu^0 is present and are similar to that obtained with Cu powder. In each supported Cu catalyst, the TOF is maximized at a θ_{Cu^0} value of 0.5–0.6; therefore, optimum activity is achieved when Cu^0 and Cu^{+1} sites coexist on the catalyst surface in approximately equal amounts. With the presumption that Cu^0 species alone are involved in activating H_2, such an augmentation of the TOF is attributed to Cu^{+1} species enhancing the reactivity of CROALD. A comparison of DRIFTS spectra of CROALD adsorption on these two types of Cu sites (Fig. 13) suggests a much stronger coordination with Cu^{+1} sites compared to Cu^0 sites, which implies the higher turnover rate on the Cu^{+1} phase

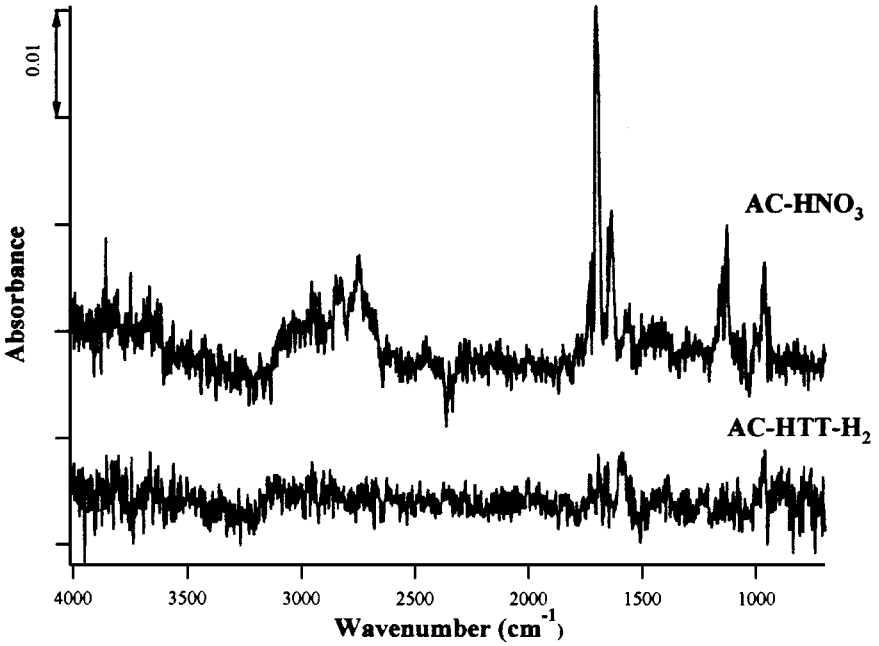

FIG. 13. DRIFTS spectra of crotonaldehyde adsorption on pure unloaded AC-HNO_3 and AC-HTT-H_2; $P_{CROALD} = 30$ Torr.

compared to metallic Cu may be due, at least partially, to a higher coverage. Significantly different adsorption behavior has been observed for CO on low index planes of Cu single crystals and Cu_2O films in terms of surface coverage (70, 71), consistent with the suggestion that the fractional coverage of Cu^{+1} sites during reaction is higher than that of Cu^0 sites owing to a stronger CROALD interaction with Cu_2O surfaces. However, differences in Cu^{+1} and Cu^0 particle size, as indicated by the XRD patterns, could also lead to significant variation in their adsorption characteristics. The latter two explanations can account for the more intense IR bands obtained during exposure of Cu^0 and Cu^{+1} surfaces to the same CROALD concentration and at the same time rationalize the higher turnover rates. The possibility of additional adsorption sites being created on the catalyst surface due to a cooperative effect between the two coexisting states of Cu cannot be discounted.

This maximization of TOF values, however, cannot explain the large enhancement in turnover rates, irrespective of the reduction temperature, observed for Cu/AC-HNO_3 compared to the other Cu catalysts. In fact, Table 1 shows that the TOF over Cu/AC-HNO_3 is highest after reduction at 573 K, which gives a Cu surface that is essentially all Cu^0. As the reduction temperature is increased to 1173 K, a drastic drop in the activity at 423 K is observed, along with significant sintering of Cu crystallites as seen by the decrease in the amount of "O" adsorbed. The concurrent drop in the TOF to approach the values of the typical catalysts implies that an alternative reaction mechanism may be responsible for the higher TOFs obtained after milder reductions. One possible explanation for such a variation is the effect of an increase in metal crystallite size on a structure-sensitive reaction, as recently proposed for this reaction over Pt (80), but consistently lower TOFs occur on both significantly larger Cu particles (Cu/AC-HTT-H_2, Cu/DM, and Cu/GF-WI) and smaller Cu particles (Cu/GF-IE), thus contradicting this explanation. A detailed characterization of the pure supports used in this study (61) revealed that the amounts and the nature of surface oxygen-containing groups on AC-HNO_3 were significantly different from those on the other carbons. Thus it seems plausible to suggest the involvement of these surface functional groups in the catalytic cycle, as proposed recently by Coloma *et al*. for CROALD hydrogenation over Pt/C catalysts (100). Srinivas and Kanta Rao (101) studied the effect of diluting Pt/C catalysts with pure carbon on the specific activity for benzene hydrogenation and interpreted the observed enhancement as evidence for additional benzene hydrogenation occurring on the carbon support as a consequence of hydrogen spillover. Similar to SiO_2 and Al_2O_3, where Lewis acid sites have been associated with acceptor sites for hydrogen, oxygen functional groups with various acid strengths were associated with sites capable of accepting spilled-over hydrogen on carbon (101, 102); however, an interaction between these sites and benzene may be more likely (103, 104). To verify a possible role of hydrogen spillover in this study, the kinetics of CROALD hydrogenation were studied using three physical mixtures, with Cu/AC-HNO_3 : AC-HNO_3 ratios of 1 : 1, 1 : 4, and 1 : 9. The corresponding TOF values after reduction at 573 K, based on "O" adsorption data on undiluted Cu/AC-HNO_3, are shown in Table 6. No activity for CROALD hydrogenation on pure AC-HNO_3 was detected. As seen in Table 6, the

TABLE 6

Effect of Diluting Cu/AC Catalysts with Pure Supports on TOFs during Crotonaldehyde Hydrogenation ($P_{CROALD} = 35$ Torr, $P_{H_2} = 710$ Torr, $T_{RED} = 573$ K, $T_{RXN} = 423$ K)

Catalyst	Carbon support	Dilution ratio (catalyst : support)	TOF (s^{-1})
Cu/AC-HNO_3	AC-HNO_3	1 : 0	0.13
Cu/AC-HNO_3	AC-HNO_3	1 : 1	0.16
Cu/AC-HNO_3	AC-HNO_3	1 : 4	0.31
Cu/AC-HNO_3	AC-HNO_3	1 : 9	0.58
Cu/AC-HTT-H_2	AC-HTT-H_2	1 : 0	0.010
Cu/AC-HTT-H_2	AC-HTT-H_2	1 : 9	0.012

TOF continuously increased as the dilution ratio increased, implying the involvement of the support in the catalytic cycle. Activity was also measured for a physical mixture of Cu/AC-HTT-H_2 and pure AC-HTT-H_2 mixed in a respective ratio of 1 : 9, and no significant enhancement in the TOF was observed (64). This further substantiates the argument that surface oxygen groups on the carbon enhance the rates with the Cu/AC-HNO_3 catalyst, presumably by providing additional adsorption sites for CROALD, which can then react with spilled-over hydrogen from the Cu^0 sites.

The adsorption of CROALD on pure AC-HNO_3 and AC-HTT-H_2 samples was studied in the DRIFTS cell, and Fig. 13 exhibits the spectra of these carbon surfaces after exposure to 15 Torr CROALD at 423 K for 30 min followed by a 30-min purge. In spite of the low signal-to-noise ratios obtained, distinct absorption bands corresponding to adsorbed CROALD can be observed in the spectrum for AC-HNO_3, whereas only very weak, if any, peaks can be distinguished in the case of AC-HTT-H_2; thus the adsorption capacity for CROALD is distinctly greater with the former, more acidic support. Since the only marked difference between the properties of these two supports is the amount and nature of surface oxygen groups present, it is reasonable to propose that the higher TOF values are due to a reaction between H atoms migrating from the Cu and CROALD adsorbed on these carbon support sites. A similar enhancement in benzene hydrogenation over acidic oxides supports has been attributed to benzene adsorbed on acid sites reacting with H atoms spilled over from the metal (103, 104); thus, by analogy, the acidic functional groups present on the surface of Cu/AC-HNO_3 are proposed to interact in a similar fashion with CROALD. A comparison of the kinetic parameters for CROALD consumption over the three AC-supported Cu catalysts is given in Table 7. The apparent activation energies for all three catalysts are very similar, although slightly higher than those observed over unsupported Cu; consequently, the higher TOFs on Cu/AC-HNO_3 cannot be explained by a decrease in this kinetic parameter. However, as seen in Table 7, a large increase in the pre-exponential factor is observed with Cu/AC-HNO_3, suggesting the creation of additional active sites on this catalyst, consistent with the spillover model proposed previously.

In an additional effort to clarify the role played by acidic functional groups, TOFs for CROALD hydrogenation on Cu/AC-HNO_3 were determined after neutralizing acidic groups on the surface using an ammonium hydroxide solution (Cu/AC-HNO_3-NH_3). The activity of this catalyst at 423 K was determined after reduction at either 423 or 573 K, and the total number of Cu surface atoms was measured by CO chemisorption and N_2O decomposition as before, and the turnover frequencies on Cu/AC-HNO_3-NH_3 are compared with those on Cu/AC-HNO_3 in Table 1. The threefold decrease in the TOFs after the NH_4OH treatment further implies that the presence of acidic groups enhances the activity, presumably via a spillover mechanism involving additional sites on the support surface.

The unusually low TOFs observed on Cu/GF-IE, irrespective of the reduction temperature, are not consistent with the high percentage of Cu^0 sites after even a mild reduction at 423 K. As compared to Cu/GF-WI and the other Cu catalysts, this behavior is abnormal and may be related to the unusual morphology of Cu particles observed in this catalyst. Detailed characterization of this catalyst, discussed in the preceding paper (62), revealed a bimodal Cu particle size distribution, with larger globular aggregates existing on top of the graphitic basal planes and smaller crystallites being preferentially stabilized along the edges of these planes. With XRD patterns indicating the presence of Cu particles on the order of 40–50 nm and chemisorption indicating an average particle size of 2–3 nm, it is possible that a large fraction of these particles are actually much smaller than the average size predicted by assuming a uniform particle morphology. Modifications in the surface and electronic characteristics of very small Cu crystallites could occur which would alter the catalytic behavior of these crystallites. The adsorption mode of an α,β-unsaturated aldehyde on a metal surface is strongly dependent on the nature of the metal and the exposed crystal plane. Binding energy calculations based on a semi-empirical extended Huckel theory have shown that such

TABLE 7

Kinetic Parameters for Crotonaldehyde Hydrogenation at 423 K; $P_{CROALD} = 35$ Torr

Catalyst	TOF (s^{-1})	E_{ACT} (kcal/mol)	Pre-exponential factor, A ($s\ atm^{0.37})^{-1}$ [a]
Cu/AC-HNO_3	0.13	11.6	63,000
Cu/AC-ASIS	0.012	10.9	3,200
Cu/AC-HTT-H_2	0.01	11.8	6,200

[a] Based upon $TOF_{CROALD} = Ae^{-E/RT}P_{H_2}^{0.61}$ for Cu/AC-HNO_3 from Table 3.

aldehydes (like CROALD) are much more strongly bound on Pt(100) and Pt(110) faces and steps compared to the Pt(111) face (74). Adsorption and hydrogenation of CROALD have therefore been suggested to occur preferentially on the (100) and (110) planes and steps, whereas those on the close-packed (111) face are less facile (74). TEM studies of flat Pt particles deposited on supports on which epitaxy can occur, like graphite, have shown the Pt(111) crystal plane to dominate (105). A similar situation could exist with Cu/GF-IE, in which small Cu particles were deposited along the edges of the graphitic basal planes. As discussed (62), the 2060 cm^{-1} peak in the DRIFTS spectra of CO adsorbed on Cu/GF-IE at 173 K indicates that Cu(111) could be the preferentially exposed crystal plane in these smaller particles. Since both Cu and Pt have fcc lattice structures, similar variations could occur in the adsorption characteristics of CROALD on the Cu(111) crystal plane. One could then suggest that CROALD adsorption on the smaller Cu^0 particles in Cu/GF-IE is less favorable than that on Cu^0 crystallites in the other catalysts, thus leading to a much lower TOF at 423 K.

Another interpretation of the unusual behavior of small metal crystallites deposited on graphite is provided by Richard *et al.* (24, 25). Using information obtained from radial electron distribution in conjunction with X-ray scattering, they attributed the Pt lattice expansion observed in an ion-exchanged Pt/graphite catalyst to electron transfer from the graphite to the metal. In contrast, no such effect was observed for Pt impregnated on an amorphous carbon support or for metal particles deposited on the graphite basal plane by an incipient wetness technique. They further justified their claim on the basis of theoretical calculations which have shown that the electron distribution in very large polyaromatic layers, such as a single graphite basal plane, is heterogeneous with a higher density of negative charge at the periphery; therefore, one could expect greater electron transfer to metal aggregates fixed on the edges than to those lying on the basal plane (25, 106). It was also suggested that the electronic structure of Pt aggregates could be perturbed by the interaction with electron-donor oxygen atoms located at the edges of basal planes. A similar effect could produce the observed differences in the behavior of Cu/GF catalysts prepared by the two methods in this study. Perturbations in the electronic structure of Cu on graphitic carbon supports as the cluster size is decreased have been reported previously (11–15). The low-wavenumber IR band at 2060 cm^{-1}, associated with stabilization of CO on Cu^0, may also indicate an enhancement in the electron density of the hybrid $d+s$ valence bands of these Cu^0 particles, which can be explained by considering the nature of CO bonding with transition metals in terms of a σ-π bonding model (72). At the same time, characterization of the graphitized fibers also indicated the presence of considerable amounts of surface oxygen groups per unit area, which decompose only upon heating above 723 K (61). Interaction of the Cu particles with such groups, located along the edges of the basal planes, could be responsible for this electronic perturbation. Whatever the cause of electron transfer, the enhanced electron density on these Cu clusters would lower the probability for activation of CROALD through the C=C bond, which involves an electron transfer of π-electrons to the metal d or hybrid $d+s$ band as a first step (25, 74). Similar to the activated adsorption proposed on the Cu(111) plane, the inhibited adsorption due to this charge transfer effect may also account for the higher activation energy for Cu/GF-IE, leading to the lower turnover rates at 423 K.

The band at 1701 cm^{-1} in all the spectra in Fig. 8 can be assigned to the carbonyl stretch frequency of CROALD weakly adsorbed on surface Cu species through the terminal C=O bond and red-shifted by about 23 cm^{-1} from the vapor-phase species. Almost no shift occurs in the frequency of the weak peak at 2730 cm^{-1}, representing the C–H stretching vibration in terminal-CHO groups (69), thus further indicating a weak interaction between the C=O group and the surface Cu. Similarly, the peaks at 970 and 1150 cm^{-1}, which can be seen in all the spectra, are very close to the corresponding vapor-phase frequencies for CROALD and can be attributed to weakly adsorbed CROALD species on the surface (69, 70). The broad band around 1540 cm^{-1} observed after low-temperature reductions, which eventually shifts to 1602 cm^{-1}, can be assigned to the olefinic stretching frequency of CROALD and implies stronger adsorption on the catalyst surface through the C=C bond. Bands in this region have been associated with ethylene and propylene π-complexes interacting with both Cu metal and Cu^{+1} cations (70, 71), and similar complexation between the C=C bond in CROALD and surface Cu species should also give rise to bands in this region. The shift in this band position toward that for the C=C stretching frequency in vapor-phase CROALD as the reduction temperature is increased to 673 K could be a consequence of the change in the Cu oxidation state from the cuprous ion to the metallic state. The prominent adjoining peak near 1432 cm^{-1} in all the spectra in Fig. 8 has been seen before on copper chromite and is assigned to the asymmetric deformation modes of the terminal $-CH_3$ group (47). This band, which is maximized after reduction at 473 K, is much more intense in comparison to the corresponding band in the vapor-phase spectrum of CROALD; however, a similar enhancement in intensity for $-CH_3$ out-of-phase deformation modes after complexation of the adjoining C=C bond with metal atoms and cations has been reported for propene adsorption on different substrates (70, 72, 73). Formation of hydrogen bonds between the hydrogen in the $-CH_3$ group of a propene–metal π-complex and surface oxygen or hydroxyl groups, leading to a substantial perturbation of the out-of-plane CH deformations of this CH_3 group, has been invoked to explain the enhanced absorbance intensity. The

coordination of propene with a metal site has been proposed to be essential for hydrogen bond formation because no hydrogen bonding was observed after these metal sites were blocked with CO_2 (73). This implied that the geometry of the adsorbed propene species may influence the interaction of the methyl group with basic groups on the catalyst surface. Similarly, the complexation of CROALD on surface Cu species, evident from the 1540–1602 cm^{-1} bands, could lead to a possible interaction between the H atoms of the terminal CH_3 group and proton-accepting groups on the surface of the DM support. The presence of appreciable amounts of weakly acidic or basic groups on the DM surface has been demonstrated by DRIFTS and TPD (61). It is reasonable, therefore, to envision similar hydrogen bond formation between these surface groups and the H atoms in the CH_3 group of CROALD anchored to surface Cu species, which leads to the pronounced 1432 cm^{-1} band. Furthermore, the 40 cm^{-1} red shift in the small, but distinct peak at 2920 cm^{-1} which represents CH stretching modes in the $-CH_3$ group is indicative of a weakening of these CH bonds, thus favoring the proposition of hydrogen bond formation. Finally, the distinct band observed around 3026 cm^{-1} in all the spectra in Fig. 8 also lies in the region where CH_x stretching vibrations are usually witnessed. The absence of this band in the vapor-phase spectrum of CROALD, together with the fact that its position is above all the frequencies at which CH_x stretches in adsorbed CROALD are observed, implies the presence of an additional surface species with a different C–H bond. This species might correspond to a partially hydrogenated CROALD species formed by the addition of one H atom. The absence of any bands corresponding to adsorbed BUTALD, which is the primary hydrogenation product, favors the argument that this partially hydrogenated species is a stable reactive intermediate providing a detectable surface coverage and whose hydrogenation could control the overall rate of reaction.

Based on all these specific assignments for the bands observed in the spectra shown in Fig. 8, three different adsorption modes for CROALD can be envisioned to be present on these Cu catalysts in analogy to structures that have been proposed on Pt and Pd (74): (i) via the C=C bond (η_2-di_{CC}), (ii) via the C=O bond (η_2-di_{CO}), and (iii) via both C=C and C=O bonds (η_4). It is not necessary to simultaneously invoke all three structures; however, to account for all the bands seen in the spectra obtained under reaction conditions, one of the following four combinations *must* exist: (A) η_2-di_{CC} and η_2-di_{CO}, (B) η_2-di_{CC} and η_4, (C) η_2-di_{CO} and η_4, (D) η_4 alone. Addition of one H atom to CROALD adsorbed through any one of these modes can give rise to the reactive intermediate proposed above.

Before proceeding, one unresolved issue is that of the exact assignment of the 1540–1602 cm^{-1} bands representing complexation of the C=C bond with one of the three forms of surface Cu species, i.e., Cu^0, Cu^{+1}, and Cu^{+2}. DRIFTS spectra of CO adsorbed at 173 K on similarly pretreated Cu/DM surfaces along with XRD and selective chemisorption data, described in the preceding paper (62), identified a gradual transition in the oxidation state of Cu as a function of reduction temperature. However, since the surface was shown to be composed of more than one phase after each pretreatment, it is not possible to unequivocally attribute the 1540–1602 cm^{-1} bands to a single oxidation state of Cu based on this information alone.

Spectra in Fig. 9 represent CROALD adsorbed on essentially the three different oxidation states of Cu. The peaks near 970, 1150, 1432, and 1701 cm^{-1} have been previously assigned. Based on the fact that one form of surface Cu clearly predominates in each of these cases, the strong bands at 1536 and 1610 cm^{-1} in Figs. 9B and 9C can now be attributed to complexation of the C=C bond with Cu^{+1} cations and metallic Cu^0 atoms, respectively. The appearance of a weak shoulder at 1630 cm^{-1} in the case of the fully oxidized catalyst surface, along with the absence of the adjoining 1432 cm^{-1} band, is indicative of a very weak interaction between CROALD and Cu^{+2} cations. Based on this additional information, the appearance of bands at 1540 and 1602 cm^{-1} under reaction conditions on Cu/DM after reduction at 473 and 673 K, respectively, is consistent with the DRIFT spectra of CO adsorbed on these surfaces at 173 K which illustrate the presence of mostly Cu^{+1} or Cu^0 on these surfaces after the respective pretreatments. The band at 1568 cm^{-1} in the spectrum of the catalyst reduced at 573 K can thus be associated with CROALD interacting with a catalyst surface composed of both Cu^0 and Cu^{+1} sites.

The prominent band at 961 cm^{-1} in the spectrum of adsorbed CROALC (Fig. 10A) can be attributed to the C–O stretch weakened and red-shifted from its vapor-phase position near 998 cm^{-1} due to coordination of the terminal –OH group with surface Cu species (70). The strong stabilization of CROALC on Cu through the C=C bond shifts the band from 1670 cm^{-1} in the free vapor state to 1562 cm^{-1} on the catalyst. The deformation modes of the CH_2 group can be detected around 1381 cm^{-1} while the peak at 1457 cm^{-1}, whose intensity is much more enhanced compared to the gas-phase, can be associated with the asymmetric deformation modes of the terminal CH_3 group. As mentioned before, the augmented intensity of this peak can be attributed to perturbed species which are strongly anchored on the Cu surface through the C=C bond but also exhibit hydrogen bonding with the DM surface. The stretching vibrations of these CH_x bonds are visible in the 2800–3000 cm^{-1} region. An additional distinct peak can be identified at 1745 cm^{-1} in spectrum A in Fig. 10 which cannot be attributed to any vibrational mode associated with CROALC. The strong C=O stretch peak at 1744 cm^{-1} in the spectrum of adsorbed BUTALD (Fig. 11A) indicates a very weak coordination with the catalyst through the C=O bond, evident

from its very small red-shift from its vapor-phase position at 1751 cm^{-1} (Fig. 11B). Similar vibrational modes of the different CH_x bonds in BUTALD are witnessed around 1400 cm^{-1} as well as in the 2800–3000 cm^{-1} region in both the adsorbed and the vapor phase. No evidence of any additional bonding with the catalyst surface is provided by any of these bands. In contrast, a much stronger stabilization of CROALC is achieved via the C=C bond, with additional coordination with the surface through the $–CH_3$ and –OH groups. Based on the assignments made for BUTALD, the distinct peak at 1745 cm^{-1} in Fig. 10A can be clearly associate with the C=O stretching frequency of weakly adsorbed BUTALD, presumably formed after CROALC adsorption, thus providing direct evidence for isomerization of CROALC to BUTALD under these conditions.

The very low CROALC selectivities obtained with these copper catalysts are consistent with a previous analysis stating that the selectivity for hydrogenating a carbonyl group conjugated with a C=C bond is lower than that expected from the relative reactivities of isolated double bonds (107). One reason is the preferential adsorption of such α,β-unsaturated aldehydes on most metals, including, Pt, Pd, and Cu, through the C=C bond rather than the C=O bond (74, 75, 81, 107, 108). This is also evident from the DRIFT spectra of CROALD adsorption on Cu/DM discussed earlier. The fraction adsorbed via the C=O bond should favor the formation of CROALC; however, stronger adsorption of CROALC on Cu compared to BUTALD and its high reactivity to either isomerize to BUTALD or hydrogenate to BUTALC gives a near-zero selectivity to this product (74, 75, 108). When adsorption occurs through both double bonds (η_4-mode), kinetic factors promote the easier hydrogenation of the C=C bond (74, 82, 98, 109, 110) and thermodynamic considerations already favor the formation of BUTALD rather than CROALC (64), as indicated in Table 8. As pointed out before by Vannice and Sen (75), these considerations explain why so few catalysts have been found to produce CROALC from CROALD with high selectivity.

The complete hydrogenation of CROALD to BUTALC is a complex sequence composed of series and parallel reactions, including an isomerization step. Although the data given in Tables 1, 4, and 5, obtained using single component feeds, do not allow a representation of the actual simultaneous rates, certain obvious kinetic trends are worth noting. The TOFs for the hydrogenation of BUTALD are much lower than those for either isomerization or hydrogenation of CROALC on Cu/AC-HNO_3, Cu/DM, and Cu/GF-WI. In contrast, these TOFs are lower and comparable for all three reactions on Cu/GF-IE. As mentioned earlier, selectivity to CROALC rather than BUTALD is nonzero only for Cu/GF-IE. A comparison of the relative hydrogenation activities of BUTALD and CROALD in Tables 1 and 4 indicates a much higher reactivity of CROALD on the Cu/AC-HNO_3, Cu/DM, and Cu/GF-WI catalyst, whereas it is comparable over Cu/GF-IE. In contrast, a similar comparison between CROALD and CROALC indicates rates are similar on all catalysts. It is evident from the values in Tables 4 and 5 that the reactivity of CROALC is much higher than that of BUTALD over Cu/AC-HNO_3, Cu/DM, and Cu/GF-WI compared to Cu/GF-IE. This is consistent with the DRIFT spectra of CROALC and BUTALD adsorbed on Cu/DM (Figs. 10 and 11), which indicated a much stronger coordination of CROALC with Cu through the C=C bond compared to BUTALD via the C=O bond.

These observations are consistent with the hypothesis that the strongest adsorption on typical Cu catalysts occurs via the C=C double bond and therefore results in almost complete selectivity toward BUTALD. Evidence for competitive adsorption between CROALC and BUTALD is provided only by Cu/GF-IE, presumably leading to a higher selectivity toward CROALC during CROALD hydrogenation. The relatively higher selectivity for CROALC exhibited by Cu/GF-IE can be explained by invoking either of the two models proposed earlier, i.e., the geometric model suggesting a high sensitivity to the exposed crystal plane or the electronic model proposing charge transfer from the support to the metal. The dominance of the Cu(111) crystal plane in Cu/GF-IE was proposed to inhibit the overall adsorption of CROALD. Binding energy calculations on Pt have also shown that this is the only crystal plane on which adsorption through the C=O bond is preferred (74). Thus enhanced adsorption of CROALD through the C=O bond on the preferentially exposed Cu(111) plane, in conjunction with inhibited isomerization of CROALC as compared to other catalysts, can account for the shift observed in the intramolecular selectivities over Cu/GF-IE. Alternatively, enrichment in the electronic density of these Cu clusters due to an interaction with the graphite support has also been proposed to improve the adsorption and the reactivity of the C=O bond compared to the C=C bond (25, 74). The main driving force for adsorption through the carbonyl bond has been suggested to be backdonation of electrons from the metal orbitals to the π^*_{CO} orbital (74). When this π^*_{CO} orbital is shifted down, for example, by complexation with a Lewis acid promoter, the interaction is better and the adsorption stronger. The effect can also be achieved

TABLE 8

Free Energy Change (ΔG) during Crotonaldehyde Hydrogenation (in kcal/mol)

Reaction T (K)	CROALC	BUTALD
298	−7.5	−17.0
400	−5.0	−15.0
600	−1.0	−8.0
700	+1.5	−5.0

by shifting the energy levels up in the corresponding Cu orbitals by increasing the valence shell electron density via charge transfer from the support. The consequence is better backbonding into the π^*_{CO} orbital and worse donation from the π_{CC} orbital, leading to a preferred C=O adsorption on Cu/GF-IE.

In situ DRIFT spectra, obtained during CROALD hydrogenation, revealed the presence of a possible partially hydrogenated intermediate species on the catalyst surface, and clearly verified the presence of CROALD adsorbed strongly through the C=C double bond and weakly through the C=O bond. Mechanistic aspects involved in CROALD hydrogenation have been discussed in detail before (47, 75, 90, 110). It has been proposed that both BUTALD and CROALC can originate from a common adsorbed intermediate involving 1,4-adsorption of CROALD (counting the oxygen atom as 1), and subsequent 1,4-addition can lead to an enolic species that can yield either of the two products. As proposed earlier, the partially hydrogenated species observed under reaction conditions can be linked to this intermediate species whose hydrogenation rate could control the overall rate of reaction. A simple Langmuir–Hinshelwood model with hydrogenation of such an intermediate species as the rate-determining step (rds) is therefore proposed to describe CROALD hydrogenation on these Cu/C catalysts. Assuming all steps other than the rds to be quasi-equilibrated, the same general sequence of elementary steps discussed previously (47) is generated as follows:

$$\mathrm{H_2} + 2\,\mathrm{S} \overset{K_{\mathrm{H_2}}}{\rightleftharpoons} 2\,\mathrm{H\text{–}S}$$

$$\mathrm{CROALD_{(g)}} + \mathrm{S} \overset{K_{\mathrm{CROALD}}}{\rightleftharpoons} \mathrm{CROALD\text{-}S}$$

$$\mathrm{H\text{–}S} + \mathrm{CROALD\text{-}S} \overset{K^*}{\rightleftharpoons} \mathrm{HCROALD\text{-}S} + \mathrm{S}$$

$$\mathrm{H\text{–}S} + \mathrm{HCROALD\text{-}S} \overset{k_1}{\rightarrow} \mathrm{CROALC\text{-}S} + \mathrm{S}$$

$$\mathrm{H\text{–}S} + \mathrm{HCROALD\text{-}S} \overset{k_2}{\rightarrow} \mathrm{BUTALD\text{-}S} + \mathrm{S}$$

$$\mathrm{CROALC\text{-}S} \rightleftharpoons \mathrm{BUTALD\text{-}S}$$

$$\mathrm{BUTALD\text{-}S} \rightleftharpoons \mathrm{BUTALD_{(g)}} + \mathrm{S}.$$

DRIFT spectra obtained under reaction conditions support the assumption that both unreacted CROALD and monohydrogenated species are present on the surface. This yields a site balance of

$$L = [\mathrm{S}] + [\mathrm{H\text{–}S}] + [\mathrm{CROALD\text{-}S}] + [\mathrm{HCROALD\text{-}S}]$$

and results in the rate expression

$$\mathrm{Rate} = \frac{kK^*K_{\mathrm{H_2}}K_{\mathrm{CROALD}}P_{\mathrm{H_2}}P_{\mathrm{CROALD}}}{\left(1 + K_{\mathrm{H_2}}^{1/2}P_{\mathrm{H_2}}^{1/2} + K_{\mathrm{CROALD}}P_{\mathrm{CROALD}} + K^*K_{\mathrm{H_2}}^{1/2}K_{\mathrm{CROALD}}P_{\mathrm{H_2}}^{1/2}P_{\mathrm{CROALD}}\right)^2},$$

where $k = k_1 + k_2$ (k_2 predominates), and $K_{\mathrm{H_2}}$ and K_{CROALD} are equilibrium adsorption constants. The capability of this equation to fit the experimental partial pressure data for Cu/AC-HNO_3 is shown in Fig. 5, with correlation constants for the four fitting parameters being near unity, and similar fits for other catalysts are provided elsewhere (64). Table 9 lists the values of these fitting parameters for each catalyst at three reaction temperatures. To test for physical consistency, the enthalpies and entropies for H_2 and CROALD adsorption were obtained from Arrhenius plots of these adsorption constants, and these values are listed in Table 10 for all the catalysts. Representative plots for Cu/AC-HNO_3 are shown in Fig. 14. The respective enthalpies of 1.6 and 2.0 kcal/gmol obtained for H_2 and CROALD adsorption on Cu/GF-IE are consistent with other evidence for weaker chemisorption on this catalyst.

TABLE 9

Parameters Obtained from Rate Expressions for Crotonaldehyde Hydrogenation

Catalyst	T_{RXN} (K)	k (μmol/s/g)	K_{H_2} (atm^{-1})	K_{CROALD} (atm^{-1})	K^*
Cu/AC-HNO_3	343	0.58	3.0	60.8	0.20
	373	0.99	2.2	49.4	0.21
	423	1.5	1.1	38.0	0.24
Cu/DM	398	1.3	0.76	22.8	1.5
	423	1.9	0.53	19.1	1.1
	473	3.6	0.38	7.6	2.7
Cu/GF-WI	423	0.83	3.8	61.1	0.31
	473	2.1	2.7	45.6	1.1
	498	3.1	1.9	31.9	2.6
Cu/GF-IE	473	7.1	0.64	25.0	1.0
	498	14.1	0.60	22.8	1.7
	523	25.8	0.55	20.5	2.0

SUMMARY

The adsorption and catalytic behavior of Cu supported on different forms of carbons, i.e., activated carbon, graphitized carbon fibers, and diamond powder, were examined during crotonaldehyde hydrogenation. A wide variation in the specific activities as well as turnover frequencies was observed as a function of the support, pretreatment

TABLE 10

Thermodynamic and Kinetic Parameters for Crotonaldehyde Hydrogenation

Catalyst	$-\Delta H^\circ_{ad}$ (kcal/mol)		ΔS°_{ad} (cal/mol/K)		E_{RDS} (kcal/mol)
	H_2	CROALD	H_2	CROALD	
Cu/AC-HNO_3	3.9	3.3	−8.8	−2.8	5.5
Cu/DM	3.3	5.2	−8.4	−6.1	5.1
Cu/GF-WI	3.8	3.5	−6.0	−2.7	7.4
Cu/GF-IE	1.6	2.0	−4.2	−2.4	6.9

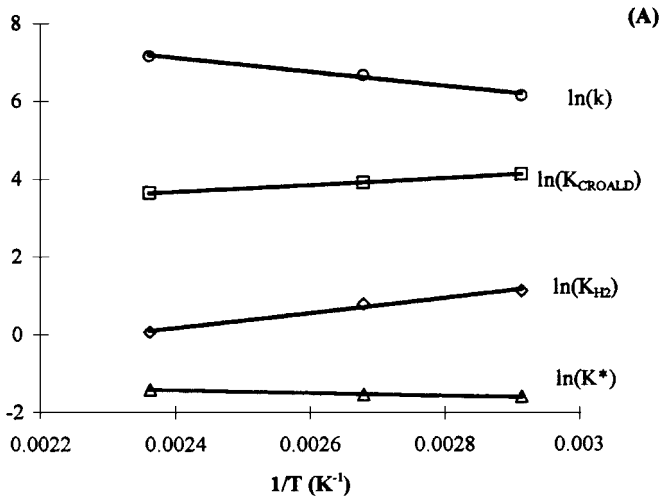

FIG. 14. Variation in the fitted kinetic parameters and adsorption equilibrium constants with temperature for Cu/AC-HNO_3.

temperature, and the catalyst preparation, technique. The TOF of each "typical" catalyst varied with the fraction of Cu sites existing as Cu^0, and the maximum TOF that occurred at a θ^0_{Cu} value of 0.5–0.6 is attributed to enhanced reactivity of CROALD adsorbed on Cu^{+1} sites. Significantly higher TOFs were observed on Cu dispersed on a nitric acid-treated activated carbon, and it is proposed that oxygen-containing acidic groups on the surface of this carbon enhance the activity by providing additional adsorption sites for CROALD which can react with hydrogen spilled over from Cu^0 sites. Unusually low TOFs exhibited by Cu deposited on the graphitized fibers by an ion-exchange technique, along with a higher selectivity toward crotyl alcohol, is rationalized by invoking either a geometric model suggesting a high sensitivity to the Cu crystal plane exposed or an electronic model proposing charge transfer from the support to small Cu particles preferentially stabilized along the edges of the graphitic basal planes. Both DRIFTS and kinetic data obtained during crotyl alcohol and butyraldehyde hydrogenation indicated stronger adsorption and higher reactivity of crotyl alcohol on Cu, thus leading to low final selectivities toward this product. *In situ* DRIFT spectra taken under reaction conditions revealed adsorbed CROALD, provided evidence for a monohydrogenated reactive intermediate with detectable surface coverage, and detected no adsorbed butyraldehyde. A Langmuir–Hinshelwood model incorporating this reaction intermediate gave an excellent fit of the kinetic data along with physically meaningful values for enthalpies and entropies of adsorption.

ACKNOWLEDGMENT

Financial support for this study was provided by the National Science Foundation via Grant CTS-9415335.

REFERENCES

1. Radovic, L. R., and Rodriguez-Reinoso, F., *Chem. Phys. Carbon* **25**, 243 (1997).
2. Stiles, A. B., "Catalyst Supports and Supported Catalysts." Butterworths, Boston, 1987.
3. Cameron, D. S., Cooper, S. J., Dodgson, I. L., Harrison, B., and Jenkins, J. W., *Catal. Today* **7**, 113 (1990).
4. Radovic, L. R., and Sudhakar, C., *in* "Introduction to Carbon Technologies" (H. Marsh, E. A. Heintz, and F. Rodriguez-Reinoso, Eds.). University of Alicante Press, Alicante, Spain, 1996.
5. Bird, A. J., *in* "Catalyst Supports and Supported Catalysts" (A. B. Stiles, Ed.). Butterworths, Boston, 1987.
6. Augustine, R. L., "Heterogeneous Catalysis for the Synthetic Chemist." Dekker, New York, 1996.
7. Rodriguez-Reinoso, F., *in* "Porosity in Carbons: Characterization and Applications" (J. W. Patrick, Ed.). Edward Arnold, London, 1995.
8. Ehrburger, P., *Adv. Colloid. Interface Sci.* **7**, 275 (1984).
9. Juntgen, H., *Fuel* **65**, 1436 (1986).
10. Leon y Leon, C. A., and Radovic, L. R., *Chem. Phys. Carbon* **24**, 213 (1996).
11. Baetzold, R. C., *Surf. Sci.* **36**, 123 (1972).
12. Carley, A. F., Rajumon, M. K., and Roberts, M. W., *J. Solid State Chem.* **106**, 156 (1993).
13. Jirka, I., *Surf. Sci.* **232**, 307 (1990).
14. De Crescenzi, M., Diociaiuti, M., Lozzi, L., Picozzi, P., Santucci, S., Battistoni, C., and Mattogno, G., *Surf. Sci.* **178**, 282 (1986).
15. Srinivasan, R., and Gopalan, P., *Surf. Sci.* **338**, 31 (1995).
16. Noronha, F. B., Schmal, M., Nicot, C., Moraweck, B., and Frety, R., *J. Catal.* **168**, 42 (1997).
17. Guerrero Ruiz, A., Lopez Gonzalez, J. D., and Rodriguez Ramos, I., *J. Chem. Soc. Chem. Common.*, 1681 (1984).
18. Phillips, J., Clausen, B., and Dumesic, J. A., *J. Phys. Chem.* **84**, 1814 (1980).
19. Medina, F., Salagre, P., Sueiras, J. E., and Fierro, J. L. G., *Appl. Catal. A* **99**, 115 (1993).
20. Nedorezova, P. M., Saratovskikh, S. L., Kolbanev, I. V., Tsvetkova, V. I., Babkina, O. N., and D'yachkovskii, F. S., *Kinet. Catal.* **31**, 151 (1990).
21. Self, V. A., and Sermon, P. A., *J. Chem. Soc. Chem. Commun.*, 834 (1990).
22. Takasu, Y., Sakuma, T., and Matsuda, Y., *Chem. Lett.*, 1179 (1985).
23. Richard, D., and Gallezot, P., *in* "Preparation of Catalysts IV" (B. Delmon, P. Grange, P. A. Jacobs, and G. Poncelet, Eds.), p. 71. Elsevier, Amsterdam, 1987.
24. Giroir-Fendler, A., Richard, D., and Gallezot, P., *in* "Heterogeneous Catalysis and Fine Chemicals" (M. Guisnet *et al.*, Eds.), p. 171. Elsevier, Amsterdam, 1988.
25. Richard, D., Gallezot, P., Neibecker, D., and Tkatchenko, I., *Catal. Today* **6**, 171 (1989).
26. Yeung, K. L., and Wolf, E. E., *J. Vac. Sci. Technol. B* **9**, 798 (1991).
27. Vannice, M. A., and Garten, R. L., *J. Catal.* **56**, 236 (1979).
28. Kuwahara, M., Ogawa, S., and Ichikawa, S., *Surf. Sci.* **344**, L1259 (1995).
29. Fournier, J., Brossard, L., Tilquin, J., Cote, R., Dodelet, J., Guay, D., and Menard, H., *J. Electrochem. Soc.* **143**, 919 (1996).
30. Imai, J., Suzuki, T., and Kaneko, K., *Catal. Lett.* **20**, 133 (1991).
31. Mahmood, T., Williams, J. O., Miles, R., and McNicol, B. D., *J. Catal.* **72**, 218 (1981).
32. Savoia, D., Trombini, C., and Umani-Ronchi, A., *Pure Appl. Chem.* **57**, 1887 (1985).
33. Baker, R. T. K., Prestridge, E. B., and Garten, R. L., *J. Catal.* **56**, 390 (1979).
34. Atamny, F., Duff, D., and Baiker, A., *Catal. Lett.* **34**, 305 (1995).

35. Lineares-Solano, A., Rodriguez-Reinoso, F., de Lecea, C. S. M., Mahajan, O. P., and Walker, P. L., Jr., *Carbon* **20**, 177 (1982).
36. Ehrburger, P., Mahajan, O. P., and Walker, P. L., Jr., *J. Catal.* **43**, 61 (1976).
37. Schlogl, R., Bowen, P., Millward, G. R., Jones, W., and Boehm, H. P., *J. Chem. Soc. Faraday Trans.* **1**, 1793 (1983).
38. Parkash, S., Chakrabarttup, S. K., and Hooley, J. G., *Carbon* **16**, 231 (1978).
39. Schlogl, R., *in* "Handbook of Heterogeneous Catalysis" (G. Ertl, H. Knözinger, and J. Weitkamp, Eds.), p. 138. Wiley–VCH, Weinheim.
40. Lambrecht, W. R. L., *Physica B* **185**, 512 (1993).
41. Pepper, S. V., *J. Vac. Sci. Technol.* **20**, 643 (1982).
42. Ryndin, Y. A., Alekseev, O. S., Simonov, P. A., and Likhilobov, V. A., *J. Mol. Catal.* **55**, 109 (1989).
43. Ryndin, Y. A., Nogin, Y. N., Paukshtis, E. A., Kalinkin, A. V., Chuvilin, A. L., and Zverev, Y. B., *J. Mol. Catal.* **62**, 45 (1990).
44. Ryndin, Y. A., Alekseev, O. S., Paukshtis, E. A., Zaikovskii, V. I., and Kalinkin, A. V., *J. Mol. Catal.* **68**, 355 (1991).
45. Bialas, H., and Niess, J., *Thin Solid Films* **268**, 35 (1995).
46. Baumann, P. K., and Nemanich, R. J., *Appl. Surf. Sci.* **104**, 267 (1996).
47. Rao, R., Dandekar, A., Baker, R. T. K., and Vannice, M. A., *J. Catal.* **171**, 406 (1997).
48. Thomas, C. L., "Catalytic Processes and Proven Catalysts." Academic Press, New York, 1970.
49. Bradley, R. H., *Appl. Surf. Sci.* **90**, 271 (1995).
50. Chen, P. A., *Thin Solid Films* **204**, 413 (1991).
51. Grzybek, T., *Polish J. Chem.* **67**, 335 (1993).
52. Kato, A., Matsuda, F., Nakajima, F., Imanari, M., and Watanabe, Y., *J. Phys. Chem.* **85**, 1710 (1981).
53. Gao, Z., and Wu, Y., *React. Kinet. Catal. Lett.* **59**, 359 (1996).
54. Nishijima, A., Kiyozumi, Y., Ueno, A., Kurita, M., Hagiwara, H., Sato, T., and Todo, N., *Bull. Chem. Soc. Jpn.* **52**, 3724 (1979).
55. Singoredjo, L., Slagt, M., Wees, J., Kapteijn, F., and Moulijn, J. A., *Catal. Today* **7**, 157 (1990).
56. Barnes, P. A., Dawson, E. A., and Midgley, G., *J. Chem. Soc. Faraday Trans.* **88**, 349 (1992).
57. Barnes, P. A., and Dawson, E. A., *J. Thermal Anal.* **41**, 621 (1994).
58. Sene, A., Jalowiecki-Duhamel, L., Wrobel, G., and Bonnelle, J. P., *J. Catal.* **144**, 544 (1993).
59. Hubaut, R., Daage, M., and Bonnelle, J. P., *Appl. Catal.* **22**, 231 (1986).
60. Li, Y., and Armor, J. N., *Appl. Catal. B* **1**, L21 (1992).
61. Dandekar, A., Baker, R. T. K., and Vannice, M. A., *Carbon* **36**, 1821 (1998).
62. Dandekar, A., Baker, R. T. K., and Vannice, M. A., *J. Catal.* **183**, 131 (1999).
63. Dandekar, A., and Vannice, M. A., submitted for publication.
64. Dandekar, A., Ph.D. dissertation, The Pennsylvania State University, 1998.
65. Madon, R. J., and Boudart, B., *I&EC Fund.* **21**, 438 (1982).
66. Dandekar, A., and Vannice, M. A., *J. Catal.* **178**, 621 (1998).
67. Kohler, M. A., Lee, J. C., Trimm, D. L., Cant, N. W., and Wainwright, M. S., *Appl. Catal.* **31**, 309 (1987).
68. Ma, J., Ph.D. thesis, The Pennsylvania State University, 1998.
69. Socrates, G., "Infrared Characteristic Group Frequencies." Wiley, Chichester, 1980.
70. Davydov, A. A., "Infrared Spectroscopy of Adsorbed Species on the Surface of Transition Metal Oxides." Wiley, London, 1990.
71. Colthup, N. B., Daly, L. H., and Wiberley, S. E., "Introduction to Infrared and Raman Spectroscopy," 3rd ed., Academic Press, San Diego.
72. Efremov, A. A., Lokhov, Y. A., and Davydov, A. A., *Kinet. Katal.* **22**, 702 (1981).
73. Efremov, A. A., and Davydov, A. A., *Kinet. Katal.* **21**, 488 (1980).
74. Delbecq, F., and Sautet, P., *J. Catal.* **152**, 217 (1995).
75. Vannice, M. A., and Sen, B., *J. Catal.* **115**, 65 (1989).
76. Noller, H., and Lin, W. M., *J. Catal.* **85**, 25 (1984).
77. Hutchings, G. J., King, F., Okoye, I. P., and Rochester, C. H., *Catal. Lett.* **23**, 127 (1994).
78. Hutchings, G. J., King, F., Okoye, I. P., Padley, M. B., and Rochester, C. H., *J. Catal.* **148**, 453 (1994).
79. Hutchings, G. J., King, F., Okoye, I. P., Padley, M. B., and Rochester, C. H., *J. Catal.* **148**, 464 (1994).
80. Englisch, M., Jentys, A., and Lercher, J. A., *J. Catal.* **166**, 25 (1997).
81. Lawrence, S. S., and Schreifels, J. A., *J. Catal.* **119**, 272 (1989).
82. Beccat, P., Bertolini, J. C., Gauthier, Y., Massardier, J., and Ruiz, P., *J. Catal.* **126**, 451 (1990).
83. Noller, H., and Lin, W. M., *React. Kinet. Catal. Lett.* **21**, 479 (1982).
84. Wismeijer, A. A., Kieboom, A. P. G., and van Bekkum, H., *React. Kinet. Catal. Lett.* **29**, 311 (1985).
85. Wismeijer, A. A., Kieboom, A. P. G., and van Bekkum, H., *Appl. Catal.* **25**, 181 (1986).
86. Banares, M., Patil, A. N., Fehlner, T. P., and Wolf, E. E., *Catal. Lett.* **34**, 251 (1995).
87. Kizling, M. B., Bigey, C., and Touroude, R., *Appl. Catal. A* **135**, L13 (1996).
88. Sokolskii, D. V., Zharmagambetova, A. K., and Anisimova, N. V., *React. Kinet. Catal. Lett.* **30**, 101 (1986).
89. Makouangou, R. M., Murzin, D. Y., Dauscher, A. E., and Touroude, R. A., *Ind. Eng. Chem. Res.* **33**, 1881 (1994).
90. Simonik, J., and Beranek, P., *Coll. Czech. Chem. Commun.* **37**, 353 (1972).
91. Simonik, J., and Beranek, P., *J. Catal.* **24**, 348 (1972).
92. Marinelli, T. B. L. W., Nabuurs, S., and Ponec, V., *J. Catal.* **151**, 431 (1995).
93. Coloma, F., Sepulveda-Escribano, A., Fierro, J. L. G., and Rodriguez-Reinoso, F., *Appl. Catal. A* **136**, 231 (1996).
94. Nagase, Y., Nakamura, H., Yazawa, Y., and Imamoto, T., *Chem. Lett.*, 927 (1992).
95. Raab, C. G., and Lercher, J. A., *J. Mol. Catal.* **75**, 71 (1992).
96. Arai, M., Obata, A., Usui, K., Shirai, M., and Nishiyama, Y., *Appl. Catal. A* **146**, 381 (1996).
97. Raab, C. G., and Lercher, J. A., *Catal. Lett.* **18**, 99 (1993).
98. Jentys, A., Englisch, M., Haller, G. L., and Lercher, J. A., *Catal. Lett.* **21**, 303 (1993).
99. Rylander, P. N., "Catalytic Hydrogenation over Platinum Metals." Academic Press, New York, 1967.
100. Coloma, F., Sepulveda-Escribano, A., and Rodriguez-Reinoso, F., *Appl. Catal. A* **123**, L1 (1995).
101. Srinivas, S. T., and Kanta Rao, P., *J. Catal.* **148**, 470 (1994).
102. Noh, J. S., and Schwarz, J. A., *Carbon* **28**, 675 (1990).
103. Lin, S. D., and Vannice, M. A., *J. Catal.* **143**, 539 (1993).
104. Lin, S. D., and Vannice, M. A., *J. Catal.* **143**, 563 (1993).
105. Yacaman, M. J., and Dominguez, E. J. M., *J. Catal.* **64**, 213(1980).
106. Stein, S. E., and Brown, R. L., *J. Am. Chem. Soc.* **109**, 3721 (1987).
107. Jenck, J., and Germain, J. E., *J. Catal.* **65**, 141 (1980).
108. Hubaut, T., Daage, M., and Bonnelle, J. P., *Appl. Catal.* **22**, 243 (1986).
109. Birchem, T., Pradier, C. M., Berthier, Y., and Cordier, G., *J. Catal.* **146**, 503 (1994).
110. Augustine, R. L., *Catal. Rev. Sci. Eng.* **13**, 285 (1976).